Response Letter

Dear Reviewer,

We sincerely thank you for your thoughtful, constructive, and insightful comments. Your suggestions have been invaluable in improving the clarity, scientific rigor, and mechanistic interpretation of our manuscript. In response, we have substantially revised the manuscript, incorporated additional analyses to strengthen the proposed mechanism, and provided point-by-point responses to each of your comments below. Figures are denoted as Fig. x, Fig. Sx, and Fig. Rx for the main text, Supplementary Information, and this response letter, respectively.

With best regards,

Yufei Liu, on behalf of all coauthors

Point-by-Point Replies to Reviewer #2

Liu and colleagues document results from 24 timeslice simulations with AWI-ESM over a full precession cycle, in which boundary conditions change the seasonal and hemispheric distribution of insolation. They focus on investigating how El Niño–Southern Oscillation (ENSO) variability responds to global mean-state shifts driven by orbital forcing. I think that these simulations and investigations therein are valuable. However, several questions arise while reading this version of the manuscript, so I do not think the central claims are supported by the analyses presented. I detail my claims below:

REPLY: We sincerely thank the reviewer for this thoughtful and constructive suggestion. Following the reviewer's recommendation, we have systematically restructured the manuscript and incorporated a series of additional diagnostic analyses to provide a clearer and more comprehensive understanding of the underlying mechanisms.

Specifically, we have reorganized the overall framework of the manuscript into two closely connected stages. The first stage focuses on how precessional forcing, through asymmetric continental heating, reorganizes the tropical Indo–Pacific mean state. The second stage investigates how these mean-state changes regulate ENSO variability by modifying the efficiency of air–sea coupling feedback.

To strengthen the mechanistic interpretation, we have added a comprehensive set of diagnostics in the revised manuscript **(Fig. 4)**, including precession-induced changes in key tropical Indo–Pacific mean-state characteristics, such as the Walker circulation **(Fig. R1)**, surface wind stress **(Fig. R2)**, Indo-Pacific warm pool position **(Fig. R3)**, mixed-layer depth **(Fig. R4)**, and upper-ocean stratification **(Fig. R5)**. In addition, we have introduced several diagnostics directly related to air–sea coupling processes, including westerly wind burst intensity **(Fig. R6)**, warm water volume variability in the western Pacific as an indicator of oceanic heat transport **(Fig. R7)**, and the Bjerknes feedback index **(Fig. R8)**.

Furthermore, to evaluate the robustness of our results, we performed additional ENSO event statistics, amplitude analyses, and sensitivity tests based on all 24 precession experiments using different Niño index definitions **(Fig. 1, Fig. S3, and Fig. R19–R20)**. We also added lead–lag analyses comparing the 90° and 270° precession phases **(Fig. R12)**, as well as composite analyses of El Niño events **(Fig. R13–R18)**, to further clarify the temporal evolution and physical mechanisms linking mean-state changes to ENSO variability.

Overall, we sincerely appreciate the reviewer's insightful and valuable comments. These revisions have substantially improved the organization, clarity, and scientific depth of the manuscript, allowing us to present the underlying physical mechanisms in a more coherent and comprehensive manner.

Major Comments:

The manuscript does not convincingly demonstrate a mechanistic link between asymmetric land heating and ENSO variability.

REPLY: We sincerely thank the reviewer for this valuable comment, which has helped us identify limitations in the mechanistic interpretation of the original manuscript. Following the reviewer's suggestion, we have carefully re-evaluated our previous physical interpretation and recognized that the original analysis based on moist static energy (MSE) may have overemphasized its role in regulating ENSO variability. Furthermore, we acknowledge that event-scale variations within individual simulations are not appropriate for interpreting ENSO variations arising from distinct mean-state backgrounds.

Accordingly, we have removed the previous MSE-based interpretation and revised the mechanistic framework by incorporating the well-established theoretical understanding of ENSO responses to mean-state changes. In the revised manuscript, we demonstrate that precessional forcing induces asymmetric continental heating, which reorganizes the tropical Indo–Pacific mean state and subsequently modulates ENSO variability through changes in the efficiency of Bjerknes feedback. This revision provides a more physically consistent framework for explaining how processional forcing influences ENSO variability and substantially strengthens the mechanistic interpretation of our study.

Lines 14–39 (Abstract): *"Geological records and climate modeling evidence indicate that the El Niño–Southern Oscillation (ENSO) is strongly modulated by Earth's axial precession, yet the mechanisms remain unclear due to interactions among multiple forcings. Using high-resolution climate simulations, we reconstruct ENSO variations across a full precessional cycle. Our results reveal that ENSO is more active when perihelion coincides with austral summer and aphelion with boreal summer, consistent with the orbital configuration of the present-day climate. Through diagnostics of background mean climate evolution and ENSO-related feedback processes, we propose that precession-scale modulations in ENSO variability are governed by east–west asymmetric continental warming. When perihelion occurs during austral summer and aphelion during boreal summer, pronounced warming emerges over Australia (east of the Indo-Pacific Intertropical Convergence Zone (ITCZ)), whereas relative cooling prevails over the Afro–Eurasian continents (west of the Indo-Pacific ITCZ). This east–west thermal contrast drives an eastward shift of the ITCZ and its coupled Walker circulation, accompanied by weakened trade winds, a shallower ocean mixed layer, and enhanced upper-ocean stratification. These changes reduce the thermal inertia of the warm pool, allowing even moderate climate noise to trigger the Bjerknes feedback (including wind and thermocline feedbacks), ultimately magnifying ENSO variability under precessional phases analogous to the modern configuration. Conversely, when perihelion falls in boreal summer and aphelion in austral summer, cooling over Australia and warming over Afro–Eurasian continents force westward displacements of the ITCZ and Walker circulation, strengthen trade winds, force a deeper mixed layer and reduced upper-ocean stratification, suppressing the Bjerknes feedback, thereby dampening ENSO activity during precessional phases corresponding to the Early Holocene. Proxy records from the Indo-Pacific region support these shifts in climatic regimes. This mechanism of zonal asymmetric continental warming establishes a physical link between astronomical precessional forcing and ENSO behavior, and may provide insights to improve assessments of long-term tropical climate variability."*

The central claim in this paper is that precession-forced asymmetric continental heating shifts the Indo-Pacific ITCZ and warm pool, modifies the Pacific east-west thermal contrast, and thereby changes ENSO amplitude. However, the analyses presented do not mechanistically demonstrate this proposed causal chain. What is shown more clearly is that Northern Hemisphere and Southern Hemisphere MSE, land heating, and rainfall vary differently (and perhaps somewhat anti-phased acc to Fig. 4a–b) over a precession cycle. That result, while valuable in its own right,is not sufficient to establish that these changes mechanistically control interannual ENSO variability.

REPLY: Following your suggestion, we performed additional analyses based on all 24 precession experiments **(Fig. 4)**. The results illustrate that the background climate state associated with enhanced ENSO variability is characterized by an eastward displacement of the Walker circulation and the Indo–Pacific warm pool, weakened trade winds, a shallower mixed layer, and enhanced upper-ocean stratification. Under such a mean-state condition, both wind and thermocline feedback are strengthened, leading to an increased overall gain of the Bjerknes feedback loop. The detailed results are as follows.

Walker circulation position

Following your suggestion, we further quantified the Walker circulation response using the annual-mean zonal mass stream function vertically averaged between 200 and 500 hPa based on all 24 precession experiments. The longitude of the Walker circulation center was defined as the streamfunction-weighted mean longitude of the positive streamfunction region between 100°E and 260°E. The results demonstrate a clear covariation between the zonal displacement of the Walker circulation center and Niño-3 SST variability throughout the full precession cycle **(Fig. R1)**. During the strong ENSO phase associated with the 255°–300° precession angles, the Walker circulation center shifts significantly eastward, extending beyond the multi-experiment mean position (~184°E). In contrast, during the weak ENSO phase at 75°–135° precession angles, the circulation center remains more westward and is confined within 180°–182°E. These results indicate a close correspondence between the zonal position of the Walker circulation and ENSO variability amplitude.

This relationship has a clear physical basis. Previous studies have demonstrated that changes in the tropical Pacific mean state can regulate ENSO amplitude by modifying the efficiency of air–sea coupling feedback (Fedorov and Philander, 2000; Fedorov et al., 2020). The zonal position of the Walker circulation is a key indicator of the tropical Pacific atmospheric background state, reflecting the distribution of deep convection and large-scale atmospheric overturning, and thereby influencing the atmospheric component of air–sea coupling processes (Capotondi et al., 2015). Accordingly, an eastward displacement of the Walker circulation center represents an eastward shift of the climatological convective system. This shift can relocate the region of strongest air–sea coupling toward the central and eastern Pacific, where SST anomalies can interact more efficiently with atmospheric circulation anomalies, thereby amplifying ENSO variability. Consistent with this interpretation, previous studies have shown that changes in tropical Pacific warm pool characteristics and atmospheric circulation patterns can directly regulate the frequency and evolution of extreme El Niño events (Thirumalai et al., 2024).

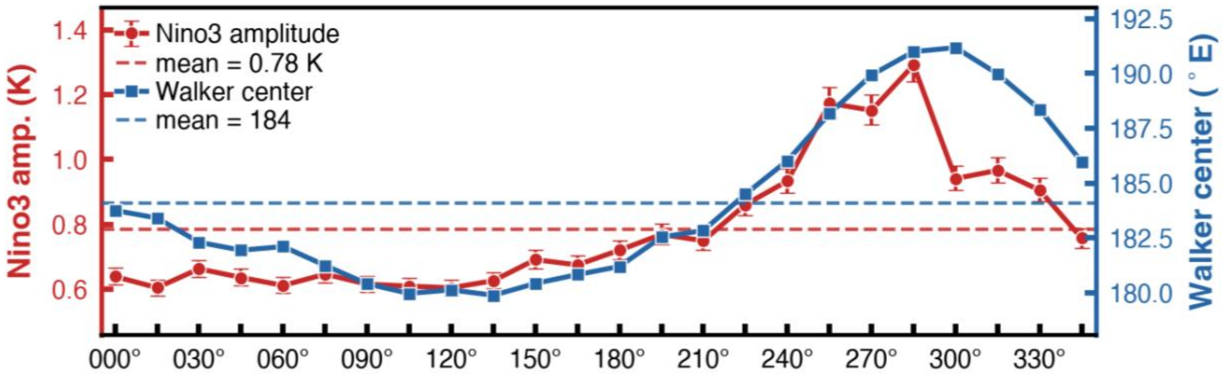

Fig. R1. Walker-circulation position and ENSO amplitude across the precession cycle. The red curve shows Niño3 amplitude with 95% confidence intervals. The blue curve shows the climatological longitude of the Walker-circulation center, defined as the streamfunction-weighted mean longitude of the positive zonal mass streamfunction within 100°–260°E after averaging over 200–500 hPa. Dashed lines indicate the corresponding 24-experiment means.

Equatorial zonal wind stress

To further investigate how the tropical circulation background state regulates ENSO variability, we followed the approach of Thirumalai et al. (2024) and selected climatological equatorial zonal wind stress as a key diagnostic metric. Based on all 24 precession experiments, we calculated the latitude-cosine-weighted regional mean of monthly zonal wind stress over the key equatorial Pacific region (5°S–5°N, 140°E–150°W). The corresponding climatological values and 95% confidence intervals were obtained from the 3-month running-mean time series. Our results reveal a clear covariation between equatorial mean zonal wind stress and Niño-3 SST amplitude throughout the full precession cycle **(Fig. R2)**. During the strong ENSO phase associated with the 255°–300° precession angles, the magnitude of negative zonal wind stress decreases, indicating weakened equatorial easterly trade winds. The wind stress values become weaker than the multi-experiment mean (~−0.056 Pa). In contrast, during the weak ENSO phase at 75°–135° precession angles, the negative zonal wind stress strengthens to approximately −0.060 to −0.061 Pa, corresponding to enhanced easterly trade winds. These phase-dependent differences demonstrate that precession-induced variations in background trade wind intensity closely correspond to changes in ENSO variability amplitude.

This relationship is also supported by previous mechanistic studies. A weakened trade wind background state, together with an eastward-shifted western Pacific warm pool, provides favorable preconditioning for the occurrence of westerly wind bursts (Eisenman et al., 2005). These atmospheric disturbances can subsequently trigger and amplify El Niño development through their influence on tropical Pacific air–sea coupling processes (Fedorov et al., 2015; Yu and Fedorov, 2022). Therefore, the enhanced ENSO variability under weakened trade wind conditions can be physically explained by the more favorable background state for westerly wind burst activity.

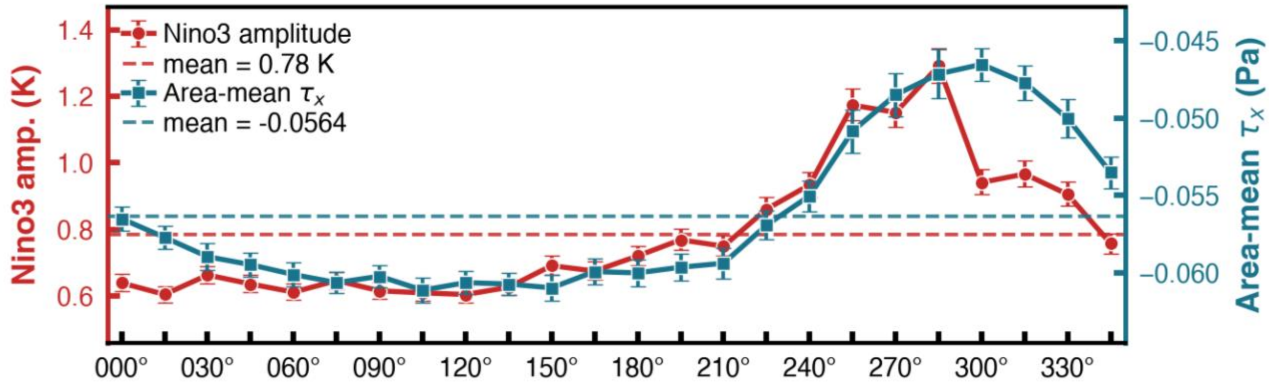

Fig. R2. Equatorial zonal wind stress and ENSO amplitude across the precession cycle. The red curve shows Niño3 amplitude. The blue curve shows the climatological area-mean zonal wind stress over 5°S–5°N, 140°E–150°W; less-negative values denote weaker easterly trades. Error bars show 95% confidence intervals, and dashed lines indicate multi-experiment means.

Extension of the IPWP

Because the IPWP is closely associated with persistent deep tropical convection, we diagnose its climatological position using the centroid longitude of tropical precipitation exceeding 5 mm day^{-1}. Across the 24 precession experiments, the IPWP centroid covaries closely with Niño3 amplitude (Fig. R3). During the strong-ENSO phases near 255°–300° (broadly in phase with the Niño3 amplitude maximum), the warm-pool centroid shifts eastward to about 136°–139°E, peaking near 139°E at 285°, relative to the multi-experiment mean position of 134°E. During the weak-ENSO phases near 75°–135°, it remains farther west, near 130°E. Thus, enhanced ENSO variability is associated with an eastward displacement of the climatological IPWP, together with an eastward Walker circulation shift and weaker equatorial trade winds.

An eastward-displaced warm pool indicates an eastward shift of the climatological convective center, which can modify the location and efficiency of tropical atmosphere–ocean coupling. Warm-pool position and the associated convective regime are important components of the tropical Pacific mean state that shape ENSO characteristics (Capotondi et al., 2015; Thirumalai et al., 2024). An eastward warm-pool background, in particular, favors a more eastward-displaced convective regime and is associated with stronger El Niño growth, including extreme events (Thirumalai et al., 2024). Consistent with this framework, the precession phases with an eastward-displaced IPWP are those with enhanced ENSO variability, suggesting that the convective background state helps modulate ENSO variability.

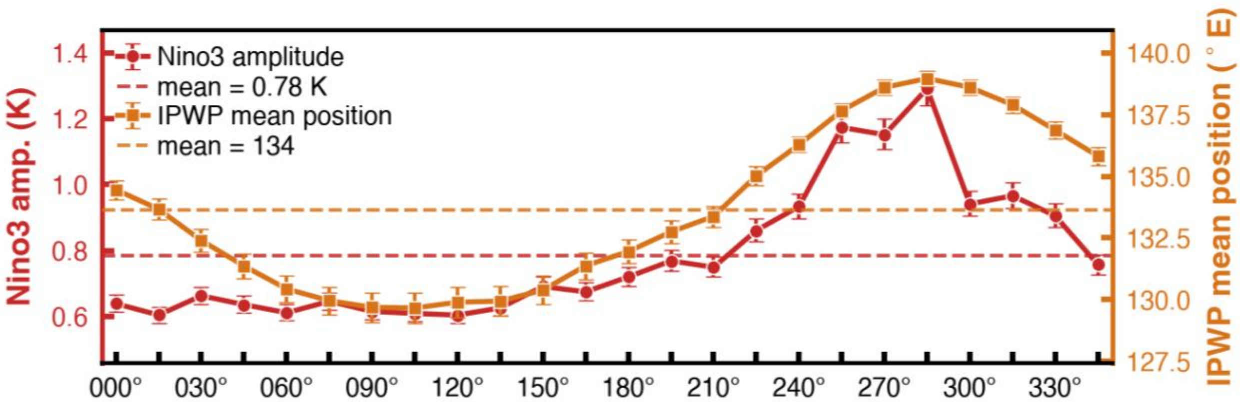

Fig. R3. Indo-Pacific warm-pool position and ENSO amplitude across the precession cycle. The red curve shows Niño3 amplitude, defined as the standard deviation of Niño3 sea surface temperature anomaly (SSTA), with 95% confidence intervals. The orange curve shows the climatological longitude of the IPWP centroid, quantified as the centroid of tropical precipitation exceeding 5 mm day^{-1}, with corresponding 95% confidence intervals. Horizontal dashed lines denote the multi-experiment means (0.78 K and 134°E).

Mixed layer depth

Having diagnosed the atmospheric mean-state changes above, we next examine the upper-ocean background conditions that regulate the oceanic response to atmospheric forcing. We diagnose the climatological mixed-layer depth (MLD) from monthly ocean temperature. At each grid point, MLD is defined using a 0.5 K temperature difference criterion relative to the surface temperature, with the crossing depth determined by linear interpolation of the native vertical profile. The monthly MLD is then area-averaged over 2.5°S–2.5°N and 140°E–150°W, and the climatological mean and 95% confidence interval are calculated from the three-month running-mean time series. Across the 24 precession experiments, climatological MLD covaries inversely with Niño3 amplitude **(Fig. R4)**. During the strong-ENSO phases near 255°–300°, the mixed layer shoals to approximately 89–94 m, reaching a minimum near 89 m at 285°, compared with the multi-experiment mean of 100 m. During the weak-ENSO phases near 75°–135°, it remains deeper, around 103–105 m. Thus, the shallowest background mixed layers occur during broadly the same precession phases characterized by an eastward Walker circulation shift, weaker trade winds, and an eastward-displaced IPWP.

A shallower mixed layer enhances the sensitivity of sea surface temperature to surface heat-flux and wind-driven forcing by reducing the effective heat capacity of the upper ocean, thereby increasing the efficiency of atmosphere–ocean coupling (Jin et al., 2006; Kim and Jin, 2011). Thirumalai et al. (2024) further highlighted shallower mixed layers as part of a tropical Pacific background state associated with stronger air–sea coupling and more extreme El Niño events. In our experiments, the phases of largest ENSO amplitude coincide with the shallowest climatological mixed layers, consistent with a precession-dependent upper-ocean background state that favors more efficient ENSO coupling.

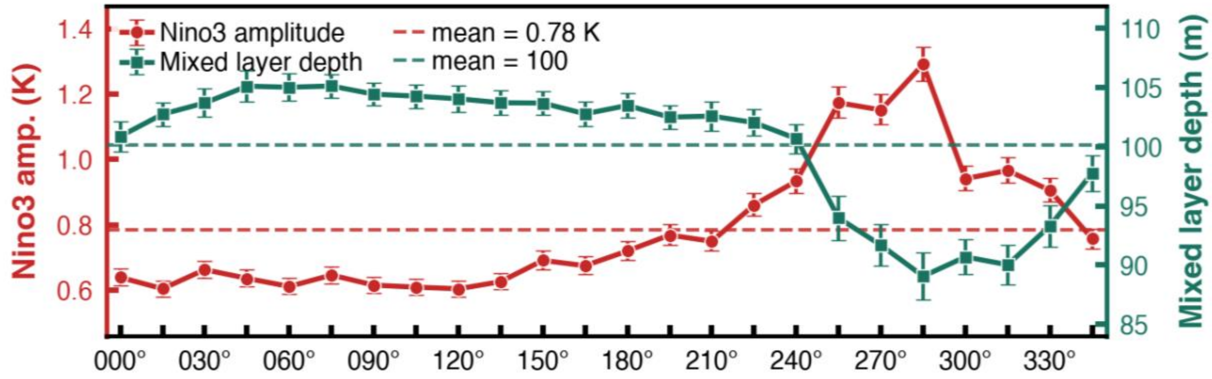

Fig. R4. Equatorial Pacific MLD and ENSO amplitude across the precession cycle. The red curve shows Niño3 amplitude, defined as the standard deviation of Niño3 SSTA, with 95% confidence intervals. The green curve shows climatological MLD averaged over 2.5°S–2.5°N, 140°E–150°W, with corresponding 95% confidence intervals. Horizontal dashed lines denote the multi-experiment means (0.78 K and 100 m).

Upper-ocean stratification

Following Cai et al. (2018), with a minor adjustment of the subsurface reference level to match our model vertical resolution, we define upper-ocean stratification as the difference between the mean temperature of the upper 100 m and the temperature at 120 m, averaged over 5°S–5°N and 140°E–150°W. Monthly values are converted to climatological means and 95% confidence intervals using the same three-month running-mean procedure as for wind stress and MLD. Across the 24 precession experiments, this stratification index covaries closely with Niño3 amplitude **(Fig. R5)**. During the strong-ENSO phases near 255°–300° (broadly in phase with the Niño3 amplitude maximum), stratification increases to approximately 1.00–1.21°C, peaking near 1.21°C at 285°, compared with the multi-experiment mean of 0.86°C. During the weak-ENSO phases near 75°–135°, it remains near or below 0.75–0.85°C. Thus, enhanced background stratification occurs during broadly the same precession phases characterized by weaker trade winds, an eastward-displaced Walker circulation, an eastward-displaced IPWP, and a shallower mixed layer.

Cai et al. (2018, 2021) showed that intensified upper-ocean stratification enhances the projection of wind-stress anomalies onto oceanic baroclinic modes, thereby amplifying SST responses associated with thermocline variations and strengthening the oceanic branch of the Bjerknes feedback. Enhanced stratification therefore favors ENSO amplification by increasing the efficiency of thermocline feedback and the sensitivity of SST to subsurface thermocline anomalies. Consistent with this mechanism, the precession phases with the strongest upper-ocean stratification in our experiments also exhibit the largest ENSO amplitude, indicating that precessional forcing modifies ENSO variability through reorganization of the coupled mean state and the associated efficiency of thermocline feedback.

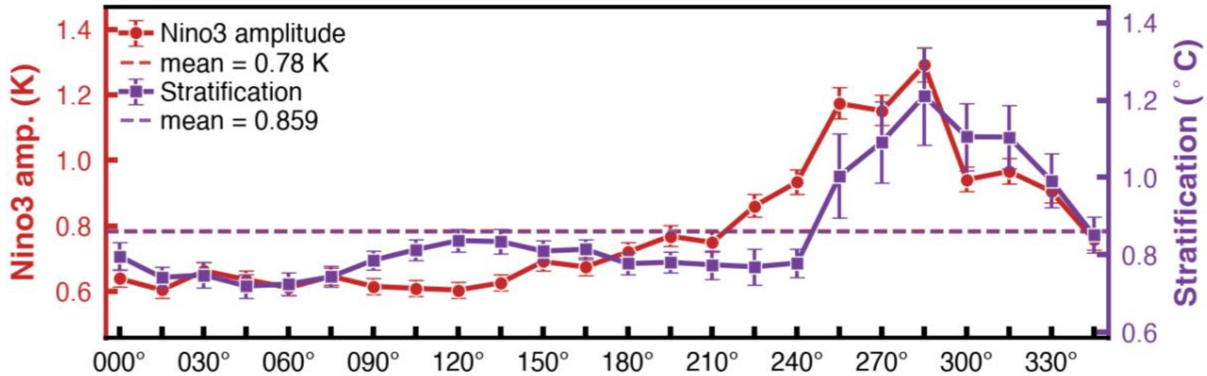

Fig. R5. Upper-ocean stratification and ENSO amplitude across the precession cycle. The red curve shows Niño3 amplitude (standard deviation of Niño3 SSTA), with 95% confidence intervals. The purple curve shows the climatological stratification index, defined as the mean temperature of the upper 100 m minus the temperature at 120 m, averaged over 5°S–5°N, 140°E–150°W (following Cai et al., 2018, with a minor reference-depth adjustment). Horizontal dashed lines denote the multi-experiment means (0.78 K and 0.86°C).

WWB intensity

WWB intensity is diagnosed from monthly zonal wind stress anomalies ($\tau x'$) averaged over 5°S–5°N, 140°E–150°W. After removing the seasonal cycle and linear trend, WWB months are defined by $\tau x' > 0.015$ Pa, and contiguous months are grouped into individual events. Event intensity is defined as the peak $\tau x'$ within each event, and we report the mean annual peak intensity together with a 95% Student's t confidence interval based on annual means ($n \approx 100$ yr). Across the precession cycle, WWB intensity exhibits a clear relationship with ENSO amplitude **(Fig. R6)**, with stronger events occurring during the strong-ENSO phases near 255°–300° (maximum ~0.026 Pa at 285°) and weaker events during the weak-ENSO phases near 75°–135°. The correlation between WWB intensity and Niño3 amplitude is approximately $r \approx 0.64$.

This relationship is consistent with the broader mean-state changes identified in our simulations. Strong-ENSO phases are characterized by an eastward-displaced Walker circulation and IPWP together with weaker climatological easterlies, conditions that favor stronger episodic westerly forcing. Because WWBs can promote ENSO development, the increase in WWB intensity indicates a more favorable coupling environment during strong-ENSO phases. We therefore interpret WWBs as part of the coupled-feedback response to mean-state changes.

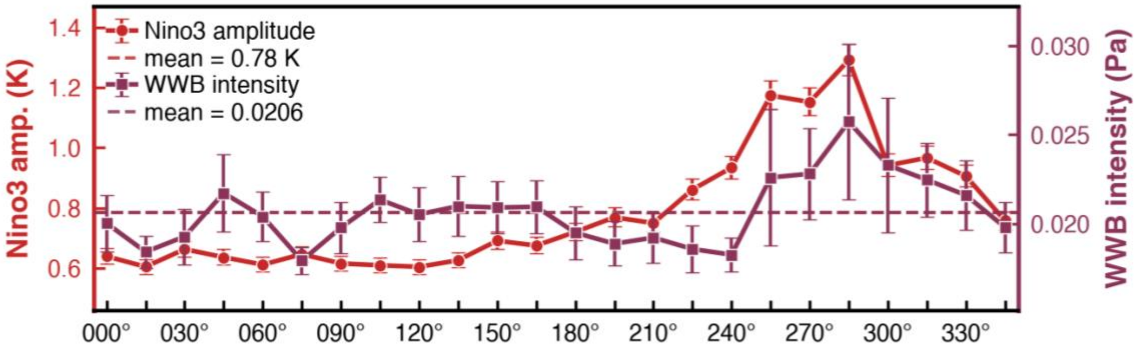

Fig. R6. WWB intensity and ENSO amplitude across the precession cycle. The red curve shows Niño3 amplitude with 95% confidence intervals. The maroon curve shows mean annual WWB peak intensity (Pa), diagnosed from deseasoned and detrended $\tau x'$ over 5°S–5°N, 140°E–150°W with threshold $\tau x' > 0.015$ Pa. Dashed lines denote multi-experiment means.

Regional warm-water volume

We define a regional warm-water volume (WWV) proxy as the climatological mean depth of the 20°C isotherm (Z20) over the western–central equatorial Pacific (5°S–5°N, 140°E–150°W). This metric characterizes variations in the equatorial thermocline and warm-water structure and is distinct from the basin-wide Meinen–McPhaden WWV index. Climatological means and 95% confidence intervals follow the same Scheme-1 procedure used for other ocean mean-state diagnostics.

The WWV exhibits a strong negative relationship with Niño3 amplitude ($r \approx -0.91$; Fig. R7), with the shallowest thermocline occurring near 285° (Z20 ≈ 166 m compared with a multi-experiment mean of ≈173 m). Stronger ENSO variability is therefore associated with a reduced equatorial warm-water reservoir and a shallower thermocline in the western–central Pacific. A shallower mean thermocline reduces upper-ocean thermal inertia and allows subsurface thermocline variations to more effectively influence sea surface temperature anomalies, thereby increasing SST sensitivity to ocean dynamical adjustments and strengthening thermocline–SST feedbacks (Jin, 1997; Meinen and McPhaden, 2000; Cai et al., 2018). This suggests that precession-induced changes in the mean thermocline state may regulate ENSO variability by modulating the efficiency of ocean–atmosphere coupling.

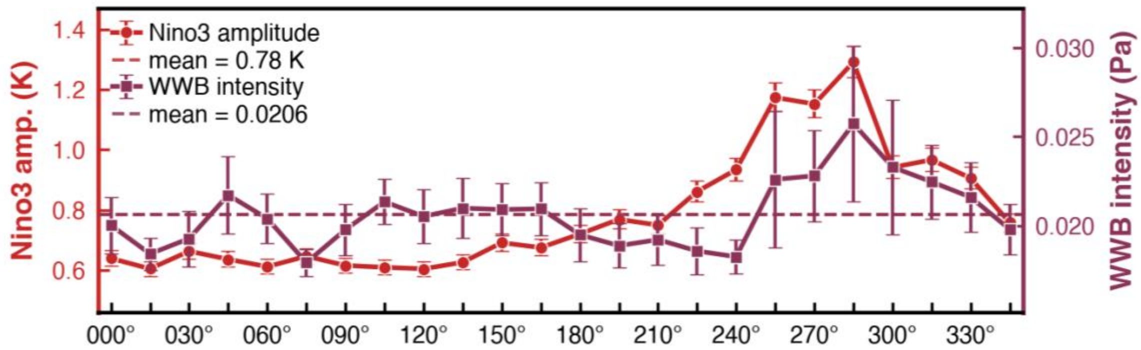

Fig. R7. Regional WWV proxy based on equatorial Z20 and ENSO amplitude across the precession cycle. The red curve shows Niño3 amplitude. The blue curve shows climatological Z20 averaged over 5°S–5°N, 140°E–150°W (lower values = shallower thermocline). Error bars show 95% confidence intervals; dashed lines denote multi-experiment means.

Atmospheric wind feedback (μ)

The Bjerknes feedback represents a key diagnostic framework for quantifying how the tropical Pacific mean state regulates the efficiency of ENSO air–sea coupling feedback. To quantitatively characterize the precessional modulation of its atmospheric component, we followed the classical regression-based approach (Lloyd et al., 2009; Okumura et al., 2011; Bellenger et al., 2014). After removing the climatological seasonal cycle, we performed a zero-lag regression between zonal wind stress anomalies over the key equatorial western Pacific region (5°S–5°N, 140°E–180°E) and Niño-3 SST anomalies. The resulting regression coefficient was defined as the atmospheric feedback parameter μ. This parameter quantifies the strength of the atmospheric response to eastern Pacific SST anomalies and provides a measure of the atmospheric coupling efficiency within the Bjerknes feedback loop.

Analysis of the 24 precession experiments shows that μ increases substantially during the 255°–300° precession interval, reaching a multi-experiment mean value of approximately 3.5×10^{-3} Pa K^{-1}, while it reaches its minimum near the 90° precession phase. These results demonstrate that the atmospheric component of the Bjerknes feedback undergoes a systematic adjustment in response to precessional forcing. However, the atmospheric feedback parameter μ alone does not fully reproduce the precessional evolution of Niño-3 variance, indicating that atmospheric coupling processes alone are insufficient to explain the complete modulation of ENSO variability under orbital-scale forcing. Therefore, we further incorporate the oceanic dynamical response term β to provide a more comprehensive assessment of the coupled air–sea feedback processes.

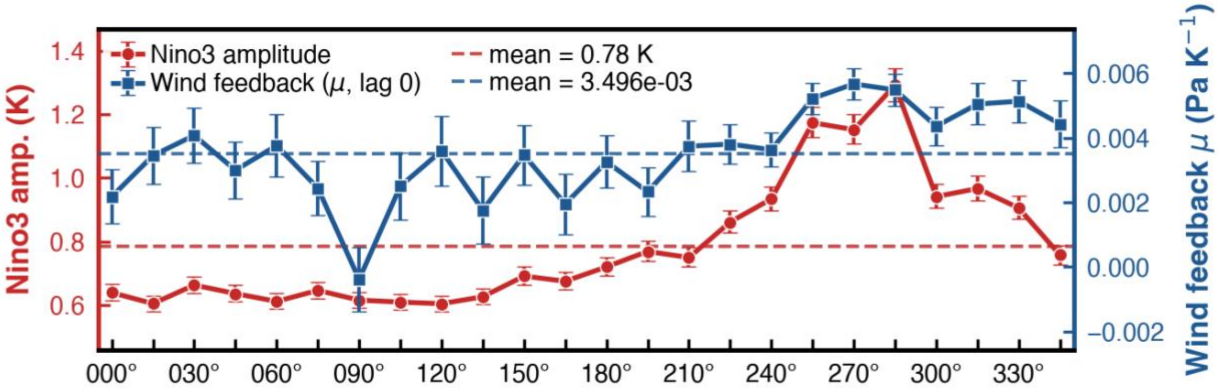

Fig. R8. Atmospheric wind feedback and ENSO amplitude across the precession cycle. The red curve shows Niño3 amplitude, with 95% confidence intervals. The blue curve shows contemporaneous wind feedback μ (Pa K^{-1}), defined from the regression of western Pacific zonal wind stress anomalies (5°S–5°N, 140°E–180°E) onto Niño3 SST anomalies. Error bars show 95% confidence intervals. Dashed lines denote multi-experiment means.

Ocean dynamical response (β)

We next examine the ocean dynamical component of the Bjerknes feedback, β. Following previous ENSO diagnostics (Deppenmeier et al., 2016; Lübbecke and McPhaden, 2013), β is defined as the regression coefficient between eastern Pacific thermocline-depth anomalies and preceding western Pacific zonal wind stress anomalies. Specifically, β is calculated by regressing Niño3-region Z_{20} anomalies (5°S–5°N, 150°W–90°W) against western Pacific zonal wind stress anomalies (5°S–5°N, 140°E–180°E). This parameter quantifies the efficiency of the wind-driven ocean dynamical response in modifying eastern Pacific thermocline conditions and represents the oceanic branch of the Bjerknes feedback (Bjerknes, 1969; Jin et al., 2006). Its magnitude depends on the tropical Pacific mean state, including background trade winds, thermocline structure, and upper-ocean stratification (DiNezio et al., 2013; Fedorov et al., 2020; Cai et al., 2018, 2021).

Across the 24 precession experiments, β exhibits pronounced orbital-scale variations (Fig. R9). It reaches a minimum near 90° (~110 m Pa^{-1}) and peaks during 255°–285° (~530–630 m Pa^{-1}), within the high-ENSO-variability interval and above the multi-experiment mean (457 m Pa^{-1}). The maximum β values generally occur at 1–2-month wind leads, consistent with the adjustment timescale of equatorial ocean dynamics. However, β alone does not fully capture the precession dependence of Niño3 variance, as indicated by the secondary maximum near 330°. These results suggest that although precessional forcing modifies the efficiency of the wind–thermocline pathway, additional feedback processes are required to explain the complete modulation of ENSO variability. Therefore, we further examine the thermocline feedback parameter α.

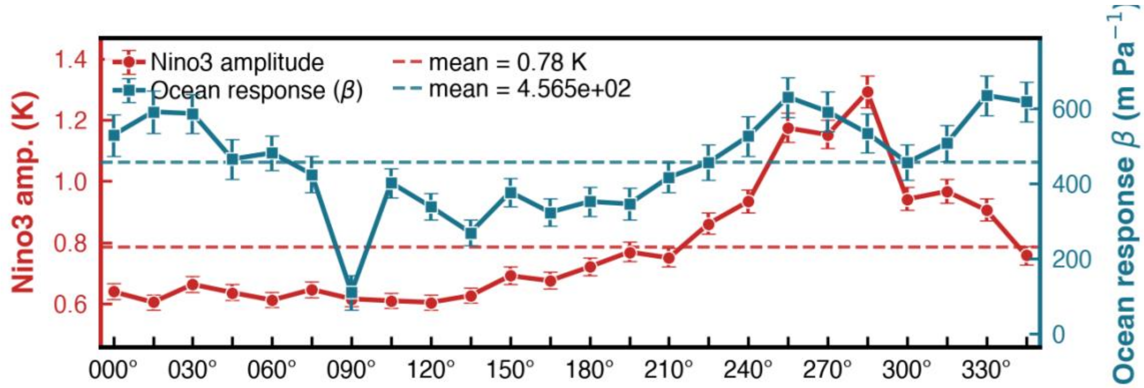

Fig. R9. Ocean dynamical response and ENSO amplitude across the precession cycle. The red curve shows Niño3 amplitude, with 95% confidence intervals. The blue curve shows the ocean response β (m Pa^{-1}), defined as the peak regression of Niño3-region Z_{20} anomalies onto western Pacific τ_x anomalies (5°S–5°N, 140°E–180°E) for wind leads of 0–6 months. Error bars show 95% confidence intervals. Dashed lines denote multi-experiment means.

Thermocline feedback (α)

We further investigate the precessional modulation of the thermocline feedback parameter α. Following previous ENSO diagnostics, α is defined as the maximum regression coefficient between Niño3 SST anomalies and preceding equatorial thermocline-depth anomalies. Specifically, monthly Z_{20} anomalies averaged over 5°S–5°N and 140°E–260°E are used to represent equatorial thermocline-depth variations, while SST anomalies over the Niño3 region (5°S–5°N, 150°W–90°W) are used to characterize eastern Pacific surface temperature changes. Thermocline anomalies are allowed to lead SST anomalies by 1–6 months, and the maximum positive regression coefficient within this period is selected as the final α value. This parameter quantifies the efficiency of thermocline–SST coupling and measures the influence of subsurface ocean anomalies on surface temperature evolution.

Previous studies have demonstrated that thermocline feedback is strongly regulated by the tropical Pacific mean state. Changes in thermocline structure, mixed-layer depth, and upper-ocean stratification can directly modify the efficiency of this feedback process (Cai et al., 2018, 2021; Thirumalai et al., 2024; Tuckman and Yang, 2026). Specifically, a deeper eastern Pacific thermocline weakens cold-water entrainment and favors positive SST anomalies, whereas a shallower thermocline enhances cold-water upwelling and promotes negative SST anomalies, thereby modulating ENSO growth and evolution (Bjerknes, 1969; Jin et al., 2006).

Across the 24 precession experiments, α exhibits pronounced orbital-scale variations (Fig. R10). During the early precession cycle, α remains relatively weak, with values of approximately 0.006–0.015 K m^{-1}. After 180°, α gradually increases and reaches a high plateau of 0.052–0.062 K m^{-1} during 225°–285°. This evolution demonstrates that changes in thermocline–SST coupling efficiency associated with upper-ocean mean-state adjustments provide an important pathway through which orbital forcing modulates ENSO variability.

The enhanced α during 225°–285° is consistent with the strengthened upper-ocean stratification and shallower mixed layer identified above, highlighting the role of background ocean conditions in regulating thermocline feedback efficiency. Together with the atmospheric feedback parameter μ and the ocean dynamical response parameter β, α completes the three-component Bjerknes feedback loop. We therefore further evaluate their combined contribution to ENSO amplification through the total feedback loop gain, BJ = μβα.

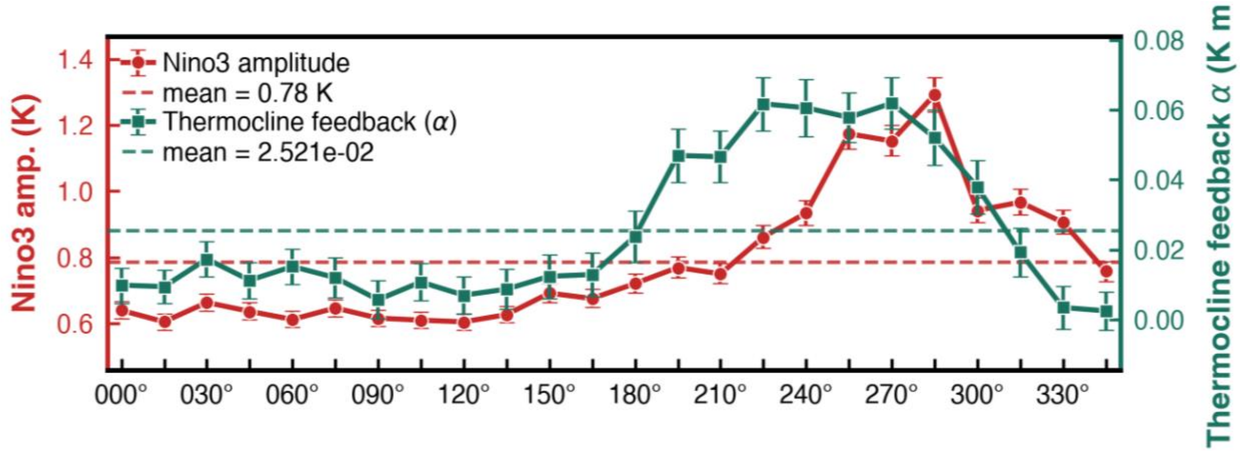

Fig. R10. Thermocline feedback and ENSO amplitude across the precession cycle. The red curve shows Niño3 amplitude, with 95% confidence intervals. The green curve shows thermocline feedback α (K m^{-1}), defined as the peak regression of Niño3 SST anomalies onto Z_{20} anomalies over 5°S–5°N, 140°E–260°E for thermocline leads of 1–6 months. Error bars show 95% confidence intervals. Dashed lines denote multi-experiment means (0.78 K and 0.025 K m^{-1}).

Total BJ (= μβα)

After quantifying the atmospheric feedback component (μ), ocean dynamical feedback component (β), and thermocline feedback component (α), we combine these three processes into a simplified Bjerknes feedback loop gain, BJ = μβα, to characterize the overall strength of the coupled air–sea feedback system.

Across the 24 precession experiments, BJ exhibits a pronounced orbital-scale evolution (Fig. R11). It remains relatively weak near the 90° precession phase, increases substantially after 180°, and reaches its maximum around 270°, with persistently elevated values during 255°–300°. Compared with the individual feedback components, the integrated feedback gain BJ provides a more consistent representation of the precession-dependent evolution of ENSO amplitude, highlighting the importance of the combined amplification of the coupled Bjerknes feedback loop.

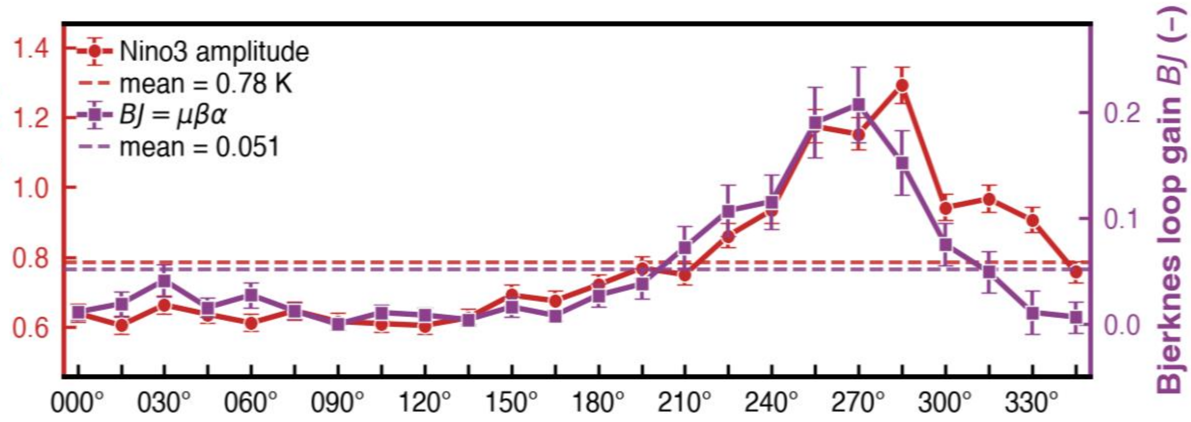

Fig. R11. Total BJ and ENSO amplitude across the precession cycle. The red curve shows Niño3 amplitude, with 95% confidence intervals. The purple curve shows the simplified loop gain BJ = μβα. Error bars show 95% confidence intervals propagated from the three components. Dashed lines denote multi-experiment means (0.78 K and 0.051).

Revision of the Original Manuscript

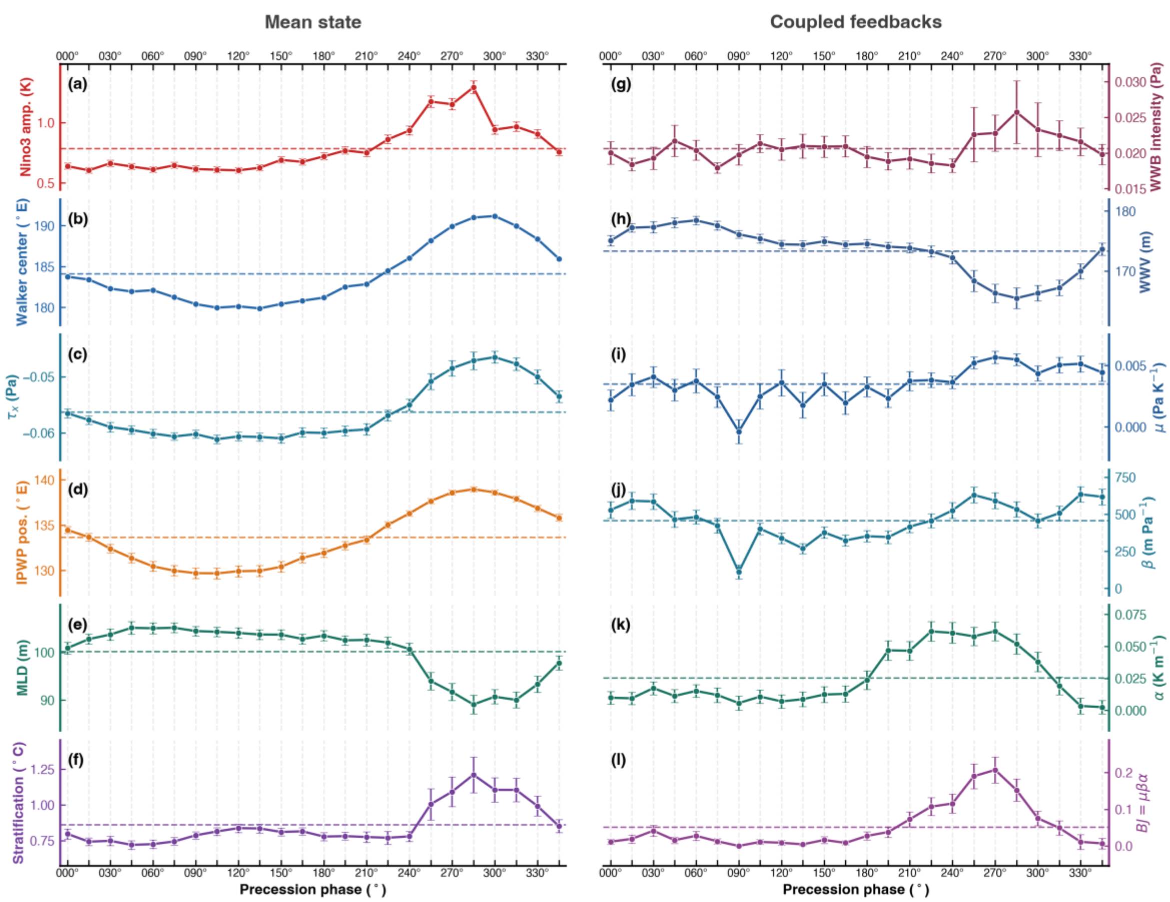

Figure 4. Mean-state and coupled-feedback diagnostics across the 24 precession experiments. Left (mean state): (a) Niño3 amplitude; (b) Walker-circulation center longitude; (c) equatorial zonal wind stress; (d) precipitation-weighted tropical convection centroid (shared ITCZ/IPWP migration surrogate); (e) mixed-layer depth; (f) upper-ocean stratification. Right (coupled feedbacks): (g) WWB intensity; (h) regional WWV proxy based on equatorial Z_{20}; (i) wind feedback μ; (j) ocean dynamical response β; (k) thermocline feedback α; (l) integrated Bjerknes loop gain BJ = μβα. Pearson correlations with Niño3 amplitude are shown in each panel. Strong-ENSO phases coincide with an eastward-displaced Walker circulation and warm pool, weaker trade winds, a shallower mixed layer, enhanced stratification, and stronger Bjerknes-loop efficiency. Definitions: Supplementary Table S3.

Lines 316–400 (Results): *"Tropical Pacific mean-state control of ENSO feedback efficiency*

Above, we have demonstrated that precession-induced asymmetric continental heating can reorganize the tropical Pacific mean state, including zonal shifts in the Walker circulation, the ITCZ, the IPWP, and changes in the equatorial thermocline structure. Building on these mean-state changes, we next investigate how the reorganized tropical Pacific background state regulates ENSO variability through changes in air–sea coupling efficiency. Previous studies have shown that ENSO variability depends not only on the magnitude of initial ocean–atmosphere disturbances, but also on the background climate state that determines the efficiency of coupled ocean–atmosphere feedback (molina2026changes, fedorov2001stability, cai2018increased). The growth of ENSO events is primarily governed by the Bjerknes positive feedback (jin2006, bjerknes1969), which consists of three interconnected processes: the atmospheric response of wind stress to SST anomalies (μ), the dynamical response of the thermocline to wind stress anomalies (β), and the thermodynamic conversion of subsurface ocean temperature anomalies associated with thermocline variations into SST anomalies (α). Together, these feedback components form a positive feedback loop that amplifies initial disturbances and promotes the growth of El Niño and La Niña events.

The efficiency of this coupled feedback is highly dependent on the location of the sensitive air–sea coupling region (wang2004understanding). The most effective coupling generally occurs near the eastern edge of the IPWP rather than within its warmest core (guilyardi2009understanding). The warm-pool interior maintains persistent deep convection, where atmospheric convection is frequently active and becomes less sensitive to small SST perturbations because it is constrained by atmospheric stability and moisture availability rather than SST forcing alone. In contrast, the eastern edge of the warm pool is located within an SST range favorable for deep convection (approximately 28°C), where relatively small SST anomalies can induce substantial changes in convection, precipitation, and latent heat release. These atmospheric responses can further modify the Walker circulation and surface wind field, which in turn regulate upper-ocean stratification and MLD and ultimately influence ENSO feedback efficiency (dinezio2012mean, fedorov2020, cai2021changing). Therefore, shifts in the zonal position of the eastern edge of the IPWP relocate the region of maximum air–sea coupling sensitivity. Such changes provide a physical pathway through which external forcing can regulate ENSO variability by modifying coupled feedback efficiency.

The 24 precession simulations reveal a clear orbital modulation of ENSO amplitude (Figure 4). During the strong ENSO phase associated with 255°–300° precession, the Walker circulation and the IPWP shift significantly eastward, accompanied by weakened equatorial easterly wind stress. These atmospheric adjustments are associated with substantial changes in upper-ocean structure, including a shallower mixed layer in the warm pool, enhanced upper-ocean stratification, and a reduced background warm-water reservoir in the western–central Pacific. These changes indicate reduced oceanic thermal inertia, which leads to enhanced sensitivity of SST anomalies to atmospheric *perturbations. Meanwhile, WWBs become stronger under this background state. The eastward displacement of the IPWP eastern edge shifts the sensitive air–sea coupling region toward the central Pacific, while the reduced oceanic thermal inertia allows the upper ocean to respond more efficiently to wind perturbations.*

Consistent with these mean-state changes, all three components of the Bjerknes feedback increase (Figure 4i–l), with the thermodynamic feedback exhibiting a particularly pronounced enhancement. The atmospheric feedback (μ) increases because SST anomalies more effectively modify atmospheric circulation and wind stress near the displaced warm-pool edge. The dynamical feedback (β) is enhanced because wind stress anomalies more efficiently perturb thermocline depth. In addition, the shallower thermocline and stronger upper-ocean stratification increase the efficiency of converting subsurface ocean temperature anomalies associated with thermocline variations into surface warming or cooling, leading to enhanced thermodynamic feedback (α). Therefore, the combined Bjerknes feedback gain (BJ = μβα) reaches its maximum near 270° precession. The strengthened positive feedback loop amplifies initial ocean–atmosphere disturbances and produces larger ENSO variability.

In contrast, ENSO variability is substantially reduced during the precessional phase between 75°–135°. The standard deviation of Niño3 SST anomalies reaches its minimum, while the Walker circulation and IPWP remain shifted westward. Stronger background easterly winds maintain a more stable cold-tongue structure and inhibit the growth of SST anomalies, while the warm pool upper ocean exhibits a deeper mixed layer, weaker stratification, and a larger thermal reservoir. Under these conditions, the efficiency of air–sea coupling decreases. The westward displacement of the IPWP eastern edge reduces the sensitivity of atmospheric convection and wind stress to SST anomalies, weakening the atmospheric feedback (μ). The reduced response of the thermocline to wind forcing decreases the dynamical feedback (β), while the deeper thermocline and weaker stratification inhibit the transfer of subsurface ocean anomalies to the surface, reducing the thermodynamic feedback (α). Consequently, the combined Bjerknes feedback gain (BJ = μβα) reaches a minimum, preventing initial disturbances from undergoing sustained amplification and resulting in weaker ENSO variability.

Together, these results demonstrate that precessional forcing does not regulate ENSO variability simply by shifting the tropical Pacific toward a mean El Niño-like or La Niña-like state. Instead, external forcing (like precession) modifies the background climate state, including the Walker circulation (dinezio2013detectability, fedorov2020), IPWP position (thirumalai2024future, molina2026changes, pontes2022mid), surface wind field, mixed-layer structure, and upper-ocean stratification (cai2018increased, tuckman2026rise), thereby regulating the efficiency of tropical Pacific air–sea coupling. These mean-state adjustments collectively modulate the three components of the Bjerknes feedback (μ, β, and α). In our simulations, enhanced upper-ocean stratification plays a particularly important role by strengthening the thermodynamic feedback (α), while the concurrent increase in atmospheric wind feedback (μ) further amplifies the total Bjerknes feedback efficiency. Together, these processes explain the enhanced ENSO variability near the 270° precession phase by establishing a background state with more efficient ocean–atmosphere coupling."

The manuscript should first distinguish how orbital forcing reorganizes the seasonal-mean tropical climate and second, how such a mean-state reorganization changes the coupled ocean-atmosphere feedbacks that generate ENSO on interannual timescales (see e.g., DiNezio et al. 2013—J.Clim; Fedorov et al. 2020—Chapter 8, ENSO in a changing climate; Pontes et al. 2022—Nat.Geosci; Thirumalai & DiNezio et al. 2024—Nature; Molina et al. 2026—J Clim; such relevant papers need to be cited and discussed, especially in the context of the mechanism proposed in the manuscript). The current manuscript largely supports the first statement, but the second remains very underexplored and is a critical limitation of the analysis presented.

REPLY: Following your suggestion, we have substantially reorganized the manuscript to clarify the distinction between the climate mean-state response to precessional forcing **and** the regulation of ENSO feedback processes by the reorganized mean state**.** Specifically, the revised manuscript now first establishes how precession-induced asymmetric continental heating reshapes the tropical Indo-Pacific mean state. The thermal contrast between the Afro-Eurasian and Australian continents generated by precessional forcing drives systematic adjustments in deep convection, the Indo-Pacific warm pool (IPWP), the Intertropical Convergence Zone (ITCZ), and the Walker circulation. These atmospheric changes further modify the equatorial trade winds and upper-ocean thermal structure. Together, these seasonal-mean atmosphere–ocean adjustments provide the background state that determines the efficiency of air–sea coupling associated with ENSO development.

In the revised manuscript, we have moved the comprehensive analysis of mean-state evolution earlier in the paper and presented this framework in the revised **Figures 2 and 3**. Building upon these mean-state changes, **Figure 4** further demonstrates how the reorganized tropical Pacific background state regulates ENSO dynamics through changes in coupled feedback processes (as described in the previous major revision response).

Lines 100–116 (Introduction): *"Yet the mechanisms linking orbital forcing, especially precession, to ENSO variability remain poorly constrained. Progress has also been limited by ENSO's high sensitivity to internal variability, the relatively weak precession signal during the Holocene that is often confounded by other forcings, and the coarse resolution of many prior simulations, which may limit the ability to capture complex equatorial current systems and active air–sea interactions in the deep tropics. Consequently, two key mechanistic questions remain unresolved: How does precession reorganize the tropical Pacific mean state? And how do those mean-state changes alter the efficiency of coupled ocean–atmosphere feedback and ultimately modulate ENSO amplitude? To address these questions, this study used state-of-the-art climate model simulations to recover ENSO activity over the entire precession cycle using unprecedentedly high-resolution simulations spanning ~10,000 years. This allows us to obtain a full picture of how precession affects ENSO behavior. In addition, given that precession is the primary driver of Holocene climate variability \cite{liu2014evolution}, we also synthesize available ENSO-sensitive proxy records across the Indo-Pacific region to corroborate the trends revealed by the simulations. With these efforts, we find that precession-forced asymmetric continental heating modulates ENSO variability by reorganizing the tropical Pacific mean state and regulating the efficiency of the coupled Bjerknes feedback loop."*

Lines 474–526 (Discussion): *"A key advance of this study is the clarification of the physical pathway through which precessional forcing reorganizes tropical mean-state conditions. Previous studies have attributed the reduced ENSO activity during the Early-Middle Holocene to a suite of tropical Pacific* *background-state changes, including intensified Asian summer monsoon circulation (liu2000modeling), an enhanced zonal Walker circulation (white2018dampened, dang2020pacific), stronger equatorial trade winds (pausata2017greening), increased eastern Pacific upwelling (white2018dampened, lu2019prominent), a westward-displaced ITCZ (pontes2022mid), an intensified zonal SST gradient (sadekov2013palaeoclimate), and enhanced subtropical warm-water subduction into the equatorial thermocline (chen2019towards, lu2025enhanced). However, these atmospheric and oceanic mean-state variables are strongly coupled and co-vary under the influence of multiple external forcings (dinezio2012mean, wang2024pdo), making it challenging to isolate the direct role of precession and determine the pathway linking orbital forcing to tropical Pacific reorganization. Based on high-resolution simulations spanning a complete precession cycle, we demonstrate that these previously identified, seemingly independent mean-state adjustments originate from a common dynamical source: precession-induced hemispheric asymmetric continental heating. This mechanism establishes a direct physical connection between orbital insolation forcing and tropical Pacific mean-state evolution, providing a unified explanation for how precession affects ENSO variability.*

Furthermore, our results demonstrate that external forcing does not regulate ENSO variability simply by shifting the mean climate state toward an El Niño-like or La Niña-like background condition (okumura2011proposed, dinezio2012mean). Instead, ENSO variability is primarily controlled through changes in the efficiency of ocean–atmosphere coupling within the tropical Pacific mean state. This mechanism shares fundamental similarities with ENSO responses under anthropogenic warming. Previous studies suggest that greenhouse warming may intensify ENSO variability by strengthening upper-ocean stratification (cai2018increased, tuckman2026rise), promoting an eastward expansion of the IPWP (thirumalai2024future, molina2026changes), weakening the Walker circulation and equatorial trade winds (dinezio2011response, dinezio2013detectability), and modifying the structure of wind stress anomalies (stuivenvolt2025widening), thereby enhancing the Bjerknes feedback and increasing the intensity and/or frequency of extreme ENSO events (dinezio2010reconciling). Although precessional forcing and anthropogenic greenhouse forcing differ fundamentally in their external origins, both influence ENSO through a common dynamical pathway: reorganizing the tropical Pacific background state and modifying the efficiency of coupled ocean–atmosphere feedback (dinezio2012mean, fedorov2020, cai2021changing). Under the 270° precession configuration, eastward migration of the IPWP and Walker circulation, decreased western–central Pacific WWV, a shallower mixed layer and intensified upper-ocean stratification reduce the thermal inertia of the western Pacific warm pool. This allows modest climatic perturbations to initiate stronger Bjerknes feedback and consequently promotes heightened ENSO variability. This explains why ENSO variability reaches its maximum amplitude under the modern-like precession configuration relative to other phases within the simulated precession cycle. Therefore, our results provide a broader perspective for understanding how variations in climate mean states regulate ENSO variability across different external forcing scenarios.

In summary, this study identifies precession-driven asymmetric continental thermal forcing as a fundamental driver of tropical Indo-Pacific mean-state reorganization and further demonstrates that changes in IPWP position, upper-ocean stratification, thermocline feedback, and the overall Bjerknes feedback system constitute key dynamical pathways through which ENSO variability responds to background climate changes. The proposed mechanism, linking orbital forcing to mean-state adjustment, air–sea coupling efficiency, and ENSO amplitude modulation, advances our understanding of astronomical-scale ENSO evolution and provides a physically based framework for interpreting ENSO responses under future climate change scenarios and associated changes in climate extremes."

A more compelling mechanistic demonstration would necessitate showing that the proposed heating asymmetry directly influences quantities involved in the time-transient and seasonally-phase-locked growth and decay of ENSO, such as Bjerknes feedback strength, surface heat-flux damping, MLD, recharge/discharge behavior, westerly wind-burst statistics, or the seasonality of coupled instability (etc.) Recent ENSO literature has emphasized these specific process-level diagnostics, including the roles of upper-ocean stratification (Tuckman and Yang, 2026—arXiv), Walker circulation strength (Fedorov et al. 2020), warm-pool westward extent (Thirumalai, DiNezio et al. 2024—Nature), and ocean-atmosphere coupling (Okumura et al. 2010—J. Clim.) in modulating ENSO amplitude and the frequency of extreme El Niño events.

REPLY: We expanded the Introduction, Results, and Discussion sections to place our mechanism within the broader framework of previous studies showing that ENSO variability responds to changes in the tropical mean state (e.g., DiNezio et al., 2013; Fedorov et al., 2020; Pontes et al., 2022; Thirumalai & DiNezio, 2024; Molina et al., 2026). Furthermore, we discuss the commonality between greenhouse-gas forcing and orbital forcing: both can influence ENSO variability by first altering the tropical mean state and subsequently modifying coupled ocean–atmosphere feedback.

Lines 86–99 (Introduction): *" In particular, weakened ENSO is thought to depend on a La Niña-like background climate (Hewitt et al., 1998; Bush et al., 1999; Sha et al., 2024), characterized by an enhanced East Asian summer monsoon (Liu et al., 2000; Liu et al., 2003; Pausata et al., 2017; Tian et al., 2017; Chen et al., 2019), strengthened Walker circulation (Bush et al., 1999), and intensified eastern Pacific upwelling (Loubere et al., 2003). More generally, previous studies have shown that external forcing reorganizes the tropical Pacific mean state through changes in Walker circulation strength (DiNezio et al., 2011; DiNezio et al., 2013), warm-pool and ITCZ shifts (Pontes et al., 2022; Thirumalai et al., 2024; Molina et al., 2026), mixed-layer depth (MLD) (Thirumalai et al., 2024), wind-stress anomaly structure (Stuivenvolt et al., 2025), and upper-ocean stratification (Cai et al., 2018; Tuckman et al., 2026). These mean-state changes regulate the efficiency of coupled ocean–atmosphere feedback that control ENSO growth, highlighting that ENSO's response to external forcing depends on the tropical Pacific mean state and multiple coupled feedback processes (DiNezio et al., 2010; DiNezio et al., 2012; Fedorov et al., 2020; Cai et al., 2021)."*

Lines 267–271 (Results): *"Therefore, consistent with previous studies, our simulations suggest that external forcing first reorganizes the tropical Pacific mean state, which provides the background conditions that regulate ENSO variability through changes in coupled ocean–atmosphere interactions (DiNezio et al., 2012; Fedorov et al., 2020; Thirumalai et al., 2024; Tuckman et al., 2026)."*

The manuscript's key point relies on Fig. 3, which shows a correlation between the east–west MSE "gap" and the Niño3 index. This is used as evidence that the zonal MSE contrast triggers positive feedback, and essentially that this correlation outlines causation. During El Niño, the warm pool shifts eastward, increasing eastern-Pacific MSE and collapsing the MSE gap, making these two measures expressions of the same event. In order to showcase causality, what is the evolution across an interannual ENSO event acc. to the model and is there evidence of the gradient leading ENSO onset over time? What forcings affect such changes? Can this be isolated to mean state changes and then precessional changes? These questions remain unanswered.

REPLY: We sincerely thank the reviewer for this valuable comment, which has helped us further improve the scientific interpretation of our study. In response to this suggestion, we performed additional lead–lag correlation analyses and El Niño composite analyses. The results indicate that the anomalous moist static energy (MSE) variations are primarily synchronized with the mature phase of ENSO events, rather than exhibiting a persistent leading signal prior to ENSO development (Fig. R12–R18).

These results suggest that statistical correlations between zonal MSE differences and the Niño3 index alone are insufficient to establish a causal relationship or to support the interpretation that MSE anomalies directly contribute to ENSO amplification. Therefore, the original manuscript's description attributing MSE evolution as a direct driver of ENSO growth was not adequately supported by the available evidence. We have accordingly removed this interpretation throughout the revised manuscript.

The updated analyses presented in the revised manuscript (Fig. 4), together with the corresponding discussion, are described in detail in our response to the major comments above.

The proposed mechanism is not clearly separated from large-scale Indo-Pacific rainfall synchronizatoin.

REPLY: We agree that large-scale Indo-Pacific rainfall synchronization is an important manifestation of the precession-induced tropical mean-state reorganization. However, it does not represent the physical mechanism directly responsible for the modulation of ENSO variability in our study.

In our framework, changes in rainfall, ITCZ position, and IPWP location represent different aspects of the tropical mean-state adjustment induced by asymmetric continental heating. The impact on ENSO variability is instead mediated by the resulting changes in upper-ocean conditions and coupled ocean–atmosphere feedback processes, including mixed-layer depth, upper-ocean stratification, and the efficiency of the Bjerknes feedback (μ, β, α, and BJ), which are quantified in the revised manuscript (Fig. 4).

To avoid this ambiguity, we have revised the manuscript to clarify that Indo-Pacific rainfall synchronization reflects large-scale mean-state reorganization, whereas changes in ENSO variability arise from the subsequent modulation of coupled ocean–atmosphere feedback.

Lines 175–188 (Methods): *"Diagnosing coupled-feedback responses to mean-state changes. To trace the pathway linking tropical Indo-Pacific mean-state reorganization to ENSO variability changes, we diagnose two sets of quantities across the 24 precession experiments (Figure 4a–l). The first set characterizes the mean-state response to precessional forcing, including the Walker-circulation center longitude, equatorial zonal wind stress (τx), ITCZ and Indo-Pacific Warm Pool (IPWP) positions, mixed-layer depth (MLD), and upper-ocean stratification (Cai et al., 2018). The second set characterizes how mean-state changes influence ENSO development. These diagnostics include westerly wind burst (WWB) intensity, a regional warm-water volume (WWV) proxy based on equatorial Z20 (depth of the 20°C isotherm), and the three components of the Bjerknes feedback together with their product (integrated Bjerknes loop gain, BJ = μβα): atmospheric wind feedback (μ), ocean dynamical response (β), and thermocline feedback (α) (Bjerknes, 1969; Jin et al., 2006; Lübbecke and McPhaden, 2013; Deppenmeier et al., 2016). Detailed definitions, calculation methods, regional domains, and uncertainty estimate for all diagnostics are provided in the Supplementary Information."*

The manuscript suggests that continental heating alters convection and the warm pool, thereby amplifying ENSO. However, the analyses do not rule out a simpler explanation: both the MSE field and Niño3 variability could be responding to a larger-scale, precession-driven reorganization of rainfall in the Indo-Pacific, the ITCZ position, and the Walker circulation. In this scenario, MSE and ENSO variability would be related but not necessarily causally connected as proposed. To address this, the authors should demonstrate lead-lag relationships among MSE anomalies, convection, zonal wind stress, thermocline depth, and Niño3 SST on interannual timescales. If MSE anomalies are mechanistically important, they should precede or modulate the atmospheric wind response that initiates ENSO growth, rather than merely covary with mature ENSO SST anomalies. Composite analyses of the El Niño onset, development, peak, and decay phases would be far more convincing than correlations across broad spatial domains. For instance, composites of precipitation, MSE, surface winds, SST, and thermocline depth during El Niño onset would help test their proposed pathway in a more direct manner.

REPLY: We sincerely thank the reviewer for this valuable comment, which has greatly helped us improve the scientific interpretation of our study. To further clarify the role of MSE variability during ENSO evolution, we performed additional event-scale diagnostics, including lead–lag correlation analyses and El Niño composite analyses, focusing on the two representative precession phases associated with weak and strong ENSO variability (90° and 270°, respectively). The results of these newly added analyses are presented in detail in the following response (Figs. R12–R18).

Lead–lag relationships during ENSO evolution

We selected the 270° and 90° experiments as representative strong- and weak-ENSO phases, respectively (near the high- and low-amplitude intervals of the precession cycle, rather than the single absolute maximum or minimum). For each experiment, we calculated lead–lag correlations over ±18 months between Niño3 SST anomalies and equatorial zonal wind stress, the zonal MSE and SST gradients, eastern- and western-Pacific Z20, and the west-minus-east Z20 difference. Before calculating the correlations, we removed the seasonal cycle and linear trend from each monthly time series, applied a three-month running mean, and standardized the resulting anomalies. We then aligned the signs of the variables according to their expected changes during El Niño. The MSE and SST gradients, western-Pacific Z20, and the west-minus-east Z20 difference decrease during El Niño and were therefore multiplied by −1. The other variables required no sign reversal. After this sign alignment, a positive correlation consistently denotes an El Niño–related change. We then identified the lag corresponding to the maximum positive correlation for each variable. Positive lags indicate that a variable leads Niño3, whereas negative lags indicate that it follows Niño3. The definitions and sign conventions of the variables used in the lead–lag analysis are summarized in Table R1.

Table R1. Definitions of the variables used in the lead–lag correlation analysis.

Variable	Definition	Sign treatment
Niño3 SST anomaly	Area-mean SSTA over 5°S–5°N, 150°W–90°W	None; reference series
Equatorial zonal wind stress	Area-mean zonal wind stress over 5°S–5°N, 140°E–150°W	None; positive anomalies indicate weaker easterly trades or stronger westerlies
Zonal MSE gradient	Western Indo-Pacific MSE minus eastern-Pacific MSE. The western region is 10°S–10°N, 60°E–140°E, and the eastern region is 5°S–5°N, 180°–100°W	Multiplied by −1; positive transformed values indicate a reduced west-minus-east gradient
Zonal SST gradient	Western Indo-Pacific SST minus eastern-Pacific SST, using the same regions as the MSE gradient	Multiplied by −1; positive transformed values indicate a reduced west-minus-east gradient
Eastern-Pacific Z20	Area-mean depth of the 20°C isotherm over 5°S–5°N, 120°W–80°W	None; positive anomalies indicate a deeper thermocline
Western-Pacific Z20	Area-mean depth of the 20°C isotherm over 5°S–5°N, 140°E–150°W	Multiplied by −1; positive transformed values indicate a shallower thermocline
West-minus-east Z20 difference	Western-Pacific Z20 minus eastern-Pacific Z20	Multiplied by −1; positive transformed values indicate a reduced west–east thermocline-depth difference

Note: All monthly time series were deseasonalized, linearly detrended, smoothed using a three-month running mean, and standardized before analysis. Variables that decrease during El Niño were multiplied by −1 so that positive correlations consistently represent El Niño–related changes. Positive lags indicate that a variable leads Niño3, whereas negative lags indicate that it follows Niño3.

Fig. R12 reveals a consistent temporal ordering in both experiments. Zonal wind stress leads Niño3 by 1–2 months, whereas the MSE and SST gradients peak nearly simultaneously with Niño3. Eastern-Pacific Z20 leads or occurs nearly simultaneously with Niño3, while the west-minus-east Z20 difference and western-Pacific Z20 lag Niño3 by approximately 1 and 4–6 months, respectively. This evolution is consistent with the rapid Bjerknes feedback response and the slower basin-scale redistribution of thermocline depth (Jin, 1997; Meinen and McPhaden, 2000). Although the temporal ordering is similar between the two experiments, the correlations are consistently stronger in the 270° experiment.

These results agree with the reviewer's interpretation that the zero-lag maxima of the MSE and SST gradients primarily reflect the mature coupled ENSO state rather than independent precursors. We have therefore removed the previous causal interpretation of the MSE gradient. However, this event-scale analysis alone does not explain how precession modulates ENSO variability across different background climates: a transient MSE anomaly does not need to precede an individual ENSO event for precession-induced mean-state changes to regulate ENSO variability.

Following the reviewer's suggestion and established ENSO theory, we further examine cross-experiment changes in climatological mean-state properties, including the Walker circulation, trade winds, warm-pool position, MLD, and upper-ocean stratification. These mean-state properties shape the background conditions that regulate ENSO feedback strength, consistent with previous studies of ENSO dynamics. The role of these precession-induced mean-state changes in modulating ENSO variability is further discussed in Fig 4.

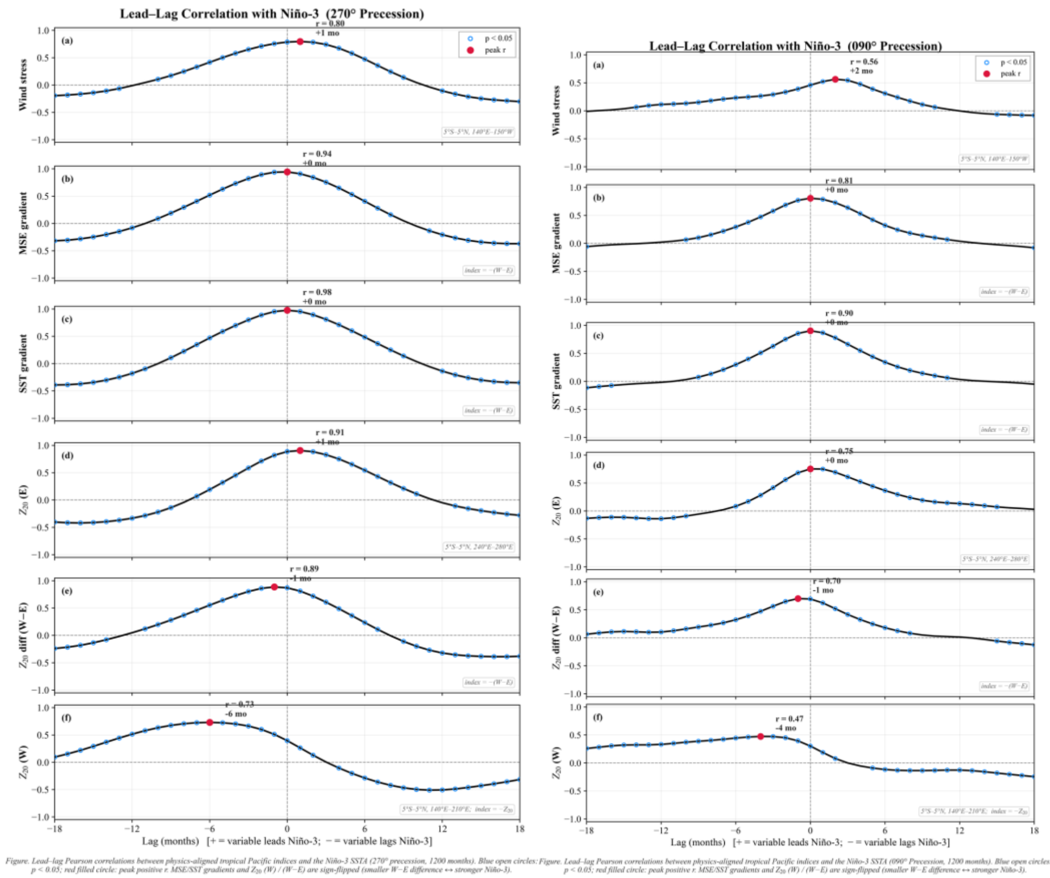

Fig. R12. Lead–lag correlations with Niño3 in the 270° and 90° experiments. The left and right columns show results for the representative strong-ENSO 270° experiment and representative weak-ENSO 90° experiment, respectively. From top to bottom, correlations are shown for equatorial zonal wind stress, the sign-adjusted west-minus-east MSE gradient, the sign-adjusted west-minus-east SST gradient, eastern-Pacific Z20, the sign-adjusted west-minus-east Z20 difference, and sign-adjusted western-Pacific Z20. Positive lags indicate that the variable leads Niño3, whereas negative lags indicate that it follows Niño3. Blue open circles denote $p < 0.05$, and red filled circles mark the maximum positive correlation.

These event-scale analyses indicate that MSE evolution is embedded within the coupled ocean–atmosphere response involving convection, Walker circulation, and thermocline adjustment.

Composite analysis

Lead–lag correlations summarize average timing but do not fully resolve the spatiotemporal evolution of ENSO. Following the reviewer's suggestion, we constructed El Niño composites for the 270° and 90° experiments, aligned to the Niño3 maximum (month 0), and examined the onset (−6 months), development (−3 months), peak (0 months), and decay (+3 months) phases. For each experiment, we combined standardized temporal evolution with spatial composites of SST, zonal wind stress, precipitation, MSE, sea-level pressure, and Z20 depth (Figs. R13–R18).

Across both experiments, the composites reveal a consistent ENSO life-cycle sequence. Anomalies in zonal wind stress, precipitation, and the Walker circulation develop before the Niño3 maximum. Eastern-Pacific SST warming and thermocline deepening peak near the mature phase, followed by a slower adjustment of the western-Pacific thermocline. This evolution is consistent with rapid Bjerknes feedback during ENSO growth and a slower basin-scale recharge–discharge response (Bjerknes, 1969; Jin, 1997; Meinen and McPhaden, 2000).

Although the overall sequence is similar, the coupled anomalies differ in strength and spatial coherence between the two experiments. In the 270° experiment, wind, convection, SST, and thermocline anomalies are already well organized during onset and intensify coherently toward the peak, with westward expansion of the eastern-Pacific warm anomaly and eastward extension of westerly wind-stress and precipitation anomalies. Near the mature phase, the SLP pattern indicates a weakened Walker circulation, and the thermocline develops the characteristic deep-eastern Pacific and shallow-western Pacific structure. In contrast, the corresponding anomalies in the 90° experiment are weaker and less organized, with a clear warm tongue and basin-scale thermocline response emerging mainly near maturity. These differences indicate stronger coupled growth under the 270° precession phase, although event composites alone cannot determine the mean-state origin of this contrast.

Consistent with the lead–lag analysis, the zonal MSE gradient decreases toward the mature phase in both experiments. We therefore interpret the transient MSE gradient as a diagnostic feature of coupled ENSO evolution rather than an independent trigger of individual events. The distinction between event-scale evolution and cross-experiment mean-state control of ENSO variability is therefore important; the latter is examined in the following response.

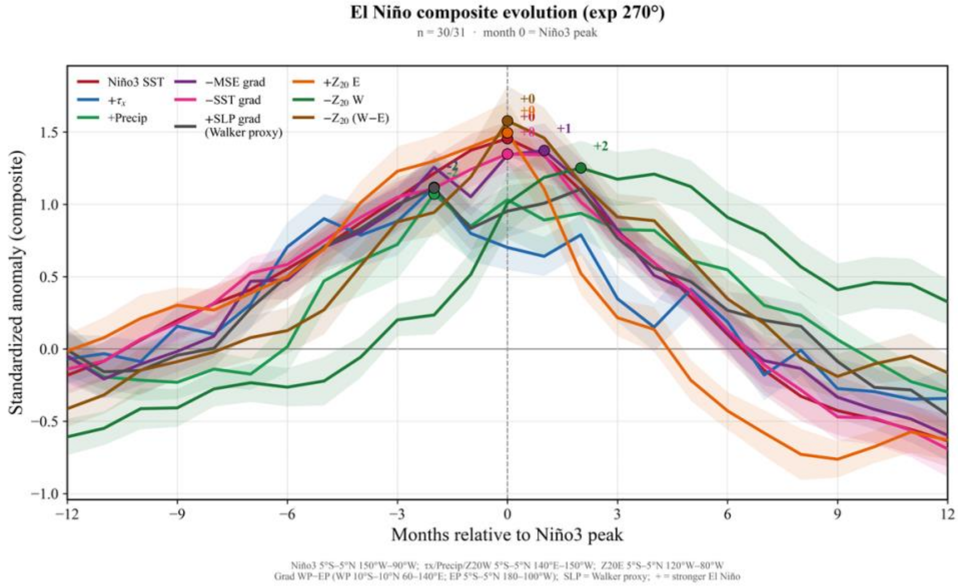

Fig. R13. Composite evolution of El Niño events in the 270° experiment. Standardized anomalies are aligned to the Niño3 peak at month 0. Curves show Niño3 SST, equatorial zonal wind stress, precipitation, the sign-adjusted MSE and SST gradients, a sea-level-pressure Walker-circulation proxy, eastern- and western-Pacific Z20, and the east–west Z20 difference. Shading denotes the inter-event standard error. The composite is based on 30 of the 31 identified El Niño events; one event near the record boundary lies outside the composite window.

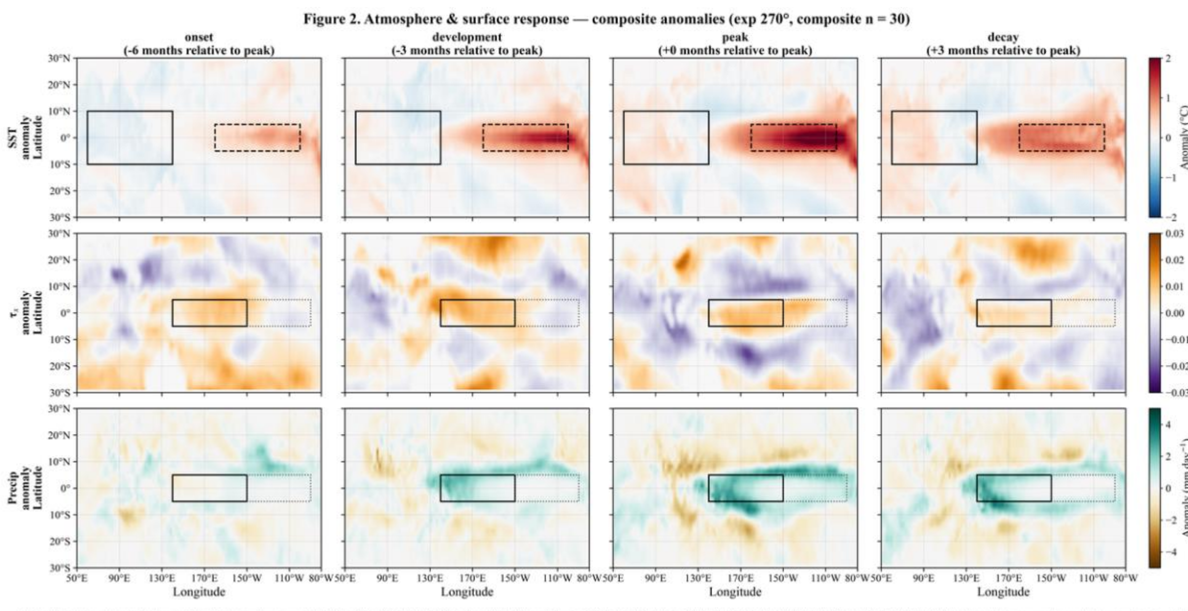

Fig. R14. Atmospheric and surface composite evolution in the 270° experiment. Columns show onset (−6 months), development (−3 months), peak (0 months), and decay (+3 months) relative to the Niño3 maximum. Rows show SST, zonal wind stress, and precipitation anomalies. Boxes delineate the regional averaging domains used to calculate the corresponding indices shown in Fig. R13.

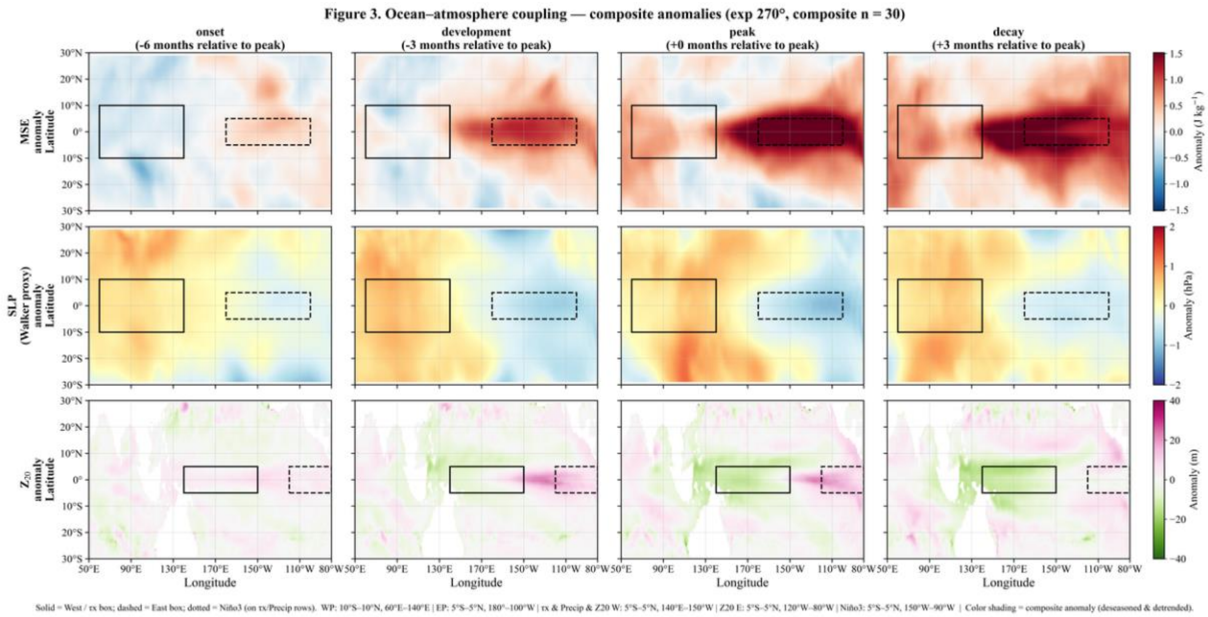

Fig. R15. Ocean–atmosphere coupling during El Niño evolution in the 270° experiment. Columns show onset, development, peak, and decay. Rows show MSE, sea-level-pressure anomalies used as a Walker-circulation proxy, and Z20 anomalies. Diagnostic boxes are the same as in Fig. R14.

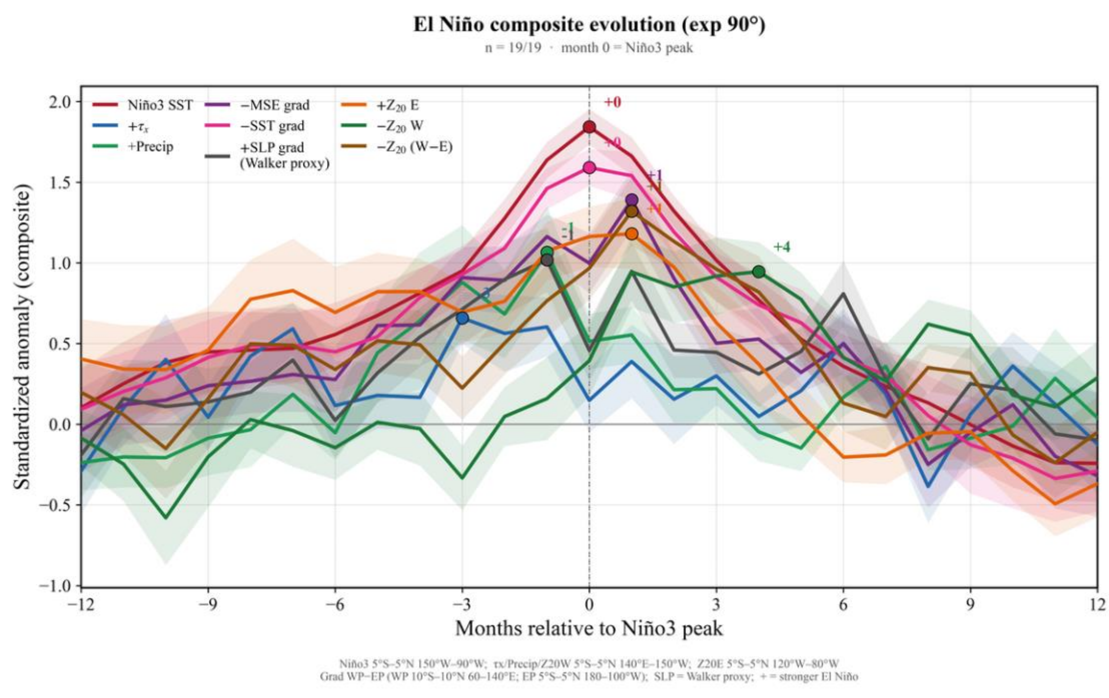

Fig. R16. Composite evolution of El Niño events in the 90° experiment. Variables and alignment follow Fig. R13. The composite is based on the 19 identified El Niño events. The smaller amplitude and broader uncertainty reflect the weaker and more irregular ENSO activity in this experiment.

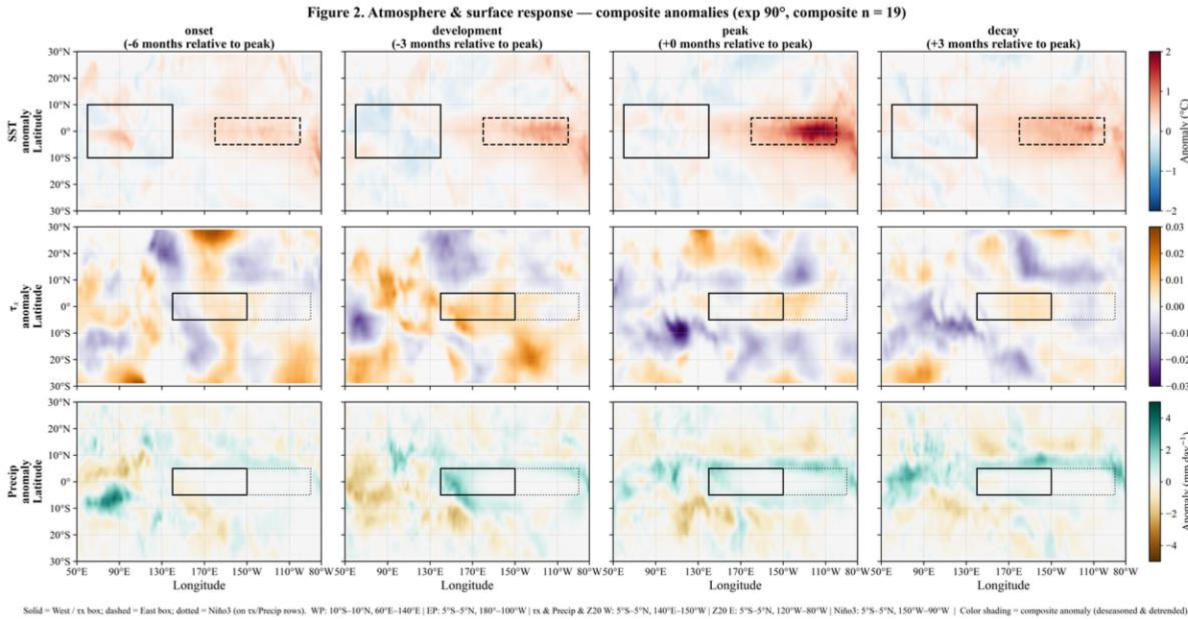

Fig. R17. Atmospheric and surface composite evolution in the 90° experiment. Columns and variables follow Fig. R14. Compared with the 270° experiment, the SST, wind-stress, and precipitation anomalies are weaker and less coherent during event growth.

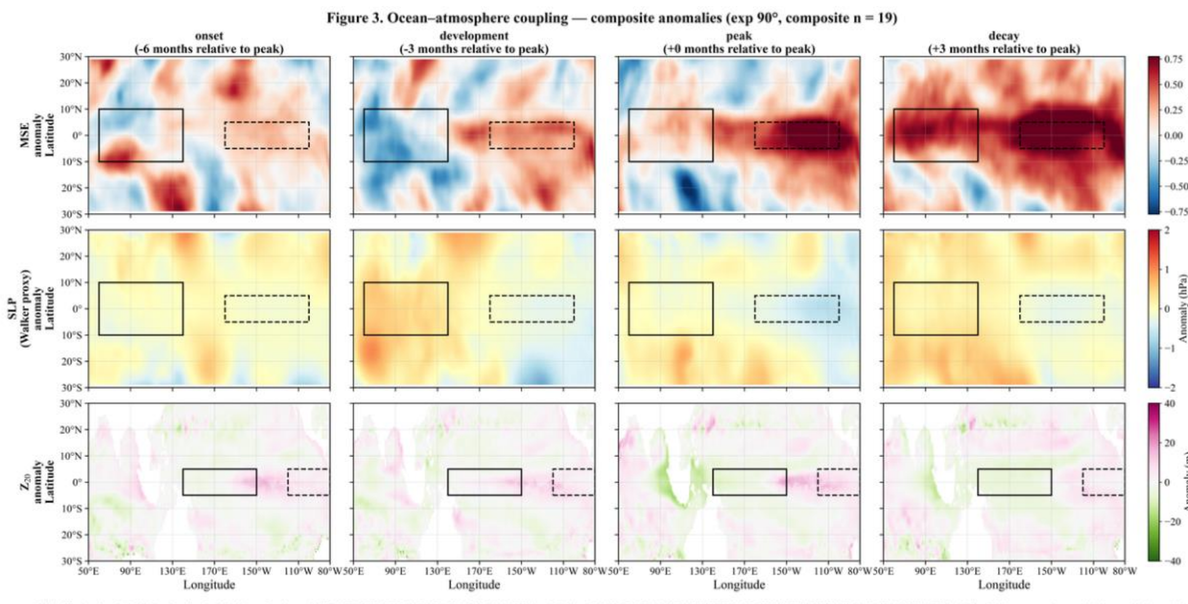

Fig. R18. Ocean–atmosphere coupling during El Niño evolution in the 90° experiment. Columns and variables follow Fig. R15. Compared with the 270° experiment, the MSE, Walker-circulation proxy, and thermocline-depth anomalies show a weaker and less organized evolution.

The contrast between the 270° and 90° experiments is therefore interpreted as a difference in the background state that regulates ENSO feedback efficiency, rather than a difference in the sequence of individual ENSO triggers.

Minor Comments:

It is unclear why Niño3 is the chosen index of focus, and not Niño3.4, as is standard for monitoring modern ENSO variability. The authors should show that this choice does not affect their conclusions.

REPLY: We sincerely thank you for this important comment, which has helped us further clarify the choice of ENSO index and strengthen the robustness of our analysis. Although the Niño3.4 index is widely used as a standard metric for characterizing modern ENSO variability, we selected the Niño3 index in this study based on two considerations. First, the model results show that the maximum center of interannual SST variability is located in the equatorial eastern Pacific (Fig. 1 and Fig. S3). This high-variability center is more closely associated with the Niño3 region than with the conventional Niño3.4 region, suggesting that the Niño3 index more directly captures the dominant ENSO-related SST variability simulated by our model. Second, we performed additional sensitivity tests using the Niño3.4 and Niño4 indices (Figs. R19–R20). These results demonstrate that the choice of ENSO index does not alter the main conclusions of this study.

Distribution of equatorial SSTA variance

Importantly, our conclusions do not depend on the choice of a single ENSO index region. We first examine the longitude–precession distribution of equatorial SSTA variance (Figure 1). The longitude-dependent variance structure shows that the precession-dependent ENSO modulation peaks in the Niño3 region.

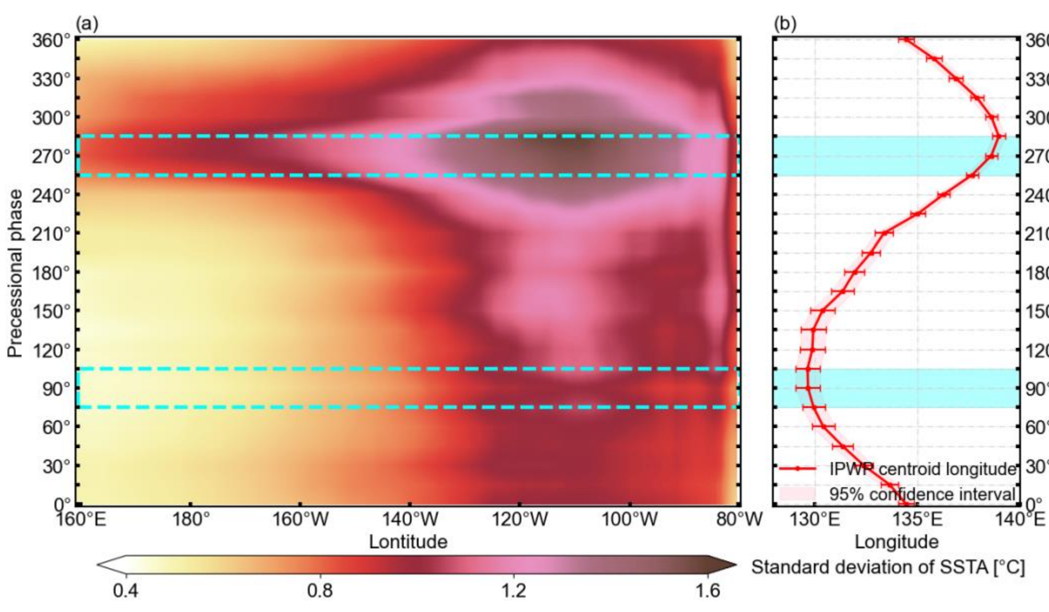

Figure 1. Longitudinal structure of ENSO variability and warm-pool position across the precession cycle. (a) Standard deviation of equatorial SSTA as a function of longitude and precession phase. Bars at the top mark the Niño3.4 and Niño3 longitude ranges. Cyan boxes mark the approximate weak-ENSO (≈75°–135°) and strong-ENSO (≈255°–300°, peak near 285°) phase ranges. (b) Climatological Indo-Pacific warm-pool centroid longitude with 95% confidence intervals.

Lines 147–149 (Methods): *"To evaluate ENSO variability across precessional phases, we first examine the longitude–precession distribution of equatorial Pacific sea surface temperature anomaly (SSTA) standard deviation (Figure 1a). Interannual variance is largest in the eastern equatorial Pacific; therefore, we use the Niño3 region (5°S–5°N, 150°W–90°W) as the primary ENSO index (Trenberth, 2001)."*

Lines 208–210 (Results): *"We find that ENSO variability is most pronounced in the Niño3 region (Figure 1a), where simulated interannual SST variance is largest in the eastern equatorial Pacific. Therefore, we use Niño3 as our primary ENSO index."*

Sensitivity tests using the Niño3.4 and Niño4 indices

In addition to the analyses based on Niño3 (Fig. S3), we performed sensitivity tests using the Niño3.4 and Niño4 indices. The same ENSO diagnostics, including event statistics, amplitude with 95% confidence intervals, power spectra, and representative time series, were recalculated using these alternative indices (Figs. R19 and R20). Both Niño3.4 and Niño4 exhibit qualitatively consistent precessional dependence with that obtained from Niño3, with stronger ENSO variability during the 240°–300° phases and weaker variability during the 60°–180° phases. These results confirm that Niño3 is a model-specific diagnostic choice based on the simulated spatial structure of ENSO variability, while the main conclusions are robust to the choice of ENSO index region.

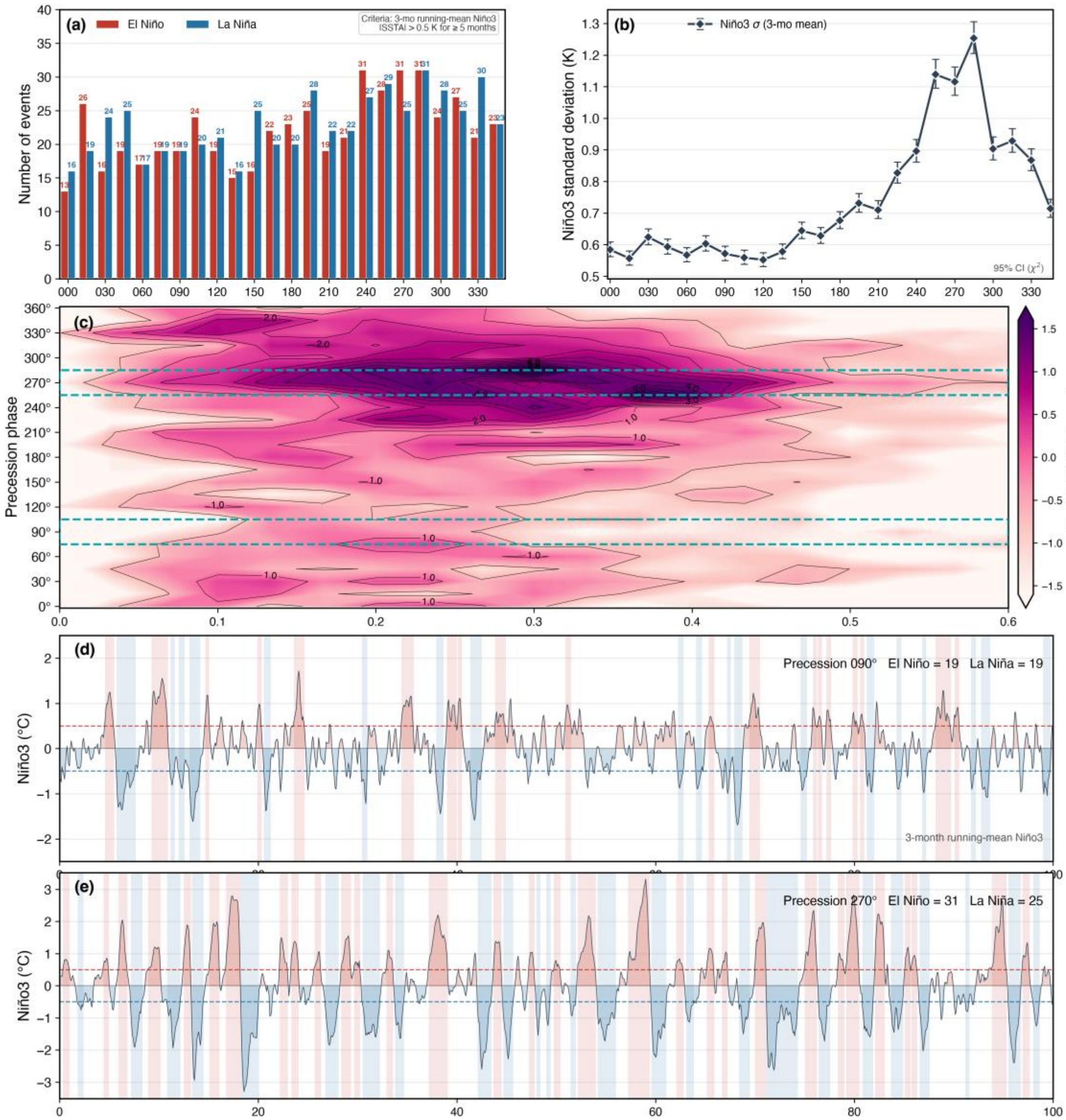

Figure S3. ENSO event occurrence and amplitude across the precession cycle. (a) Number of El Niño and La Niña events in each of the 24 experiments. Events are identified when the three-month running-mean Niño3 SSTA exceeds +0.5 K or falls below −0.5 K for at least five consecutive overlapping three-month periods. (b) Niño3 standard deviation with 95\% confidence intervals derived from the chi-square distribution. (c) Power spectral density of the Niño3 index. (d, e) Niño3 SSTA time series for the representative weak-ENSO 90° experiment and representative strong-ENSO 270° experiment, respectively. Red and blue shading indicate the identified El Niño and La Niña periods. All analyses use the final 100 years of the corresponding 400-year simulations.

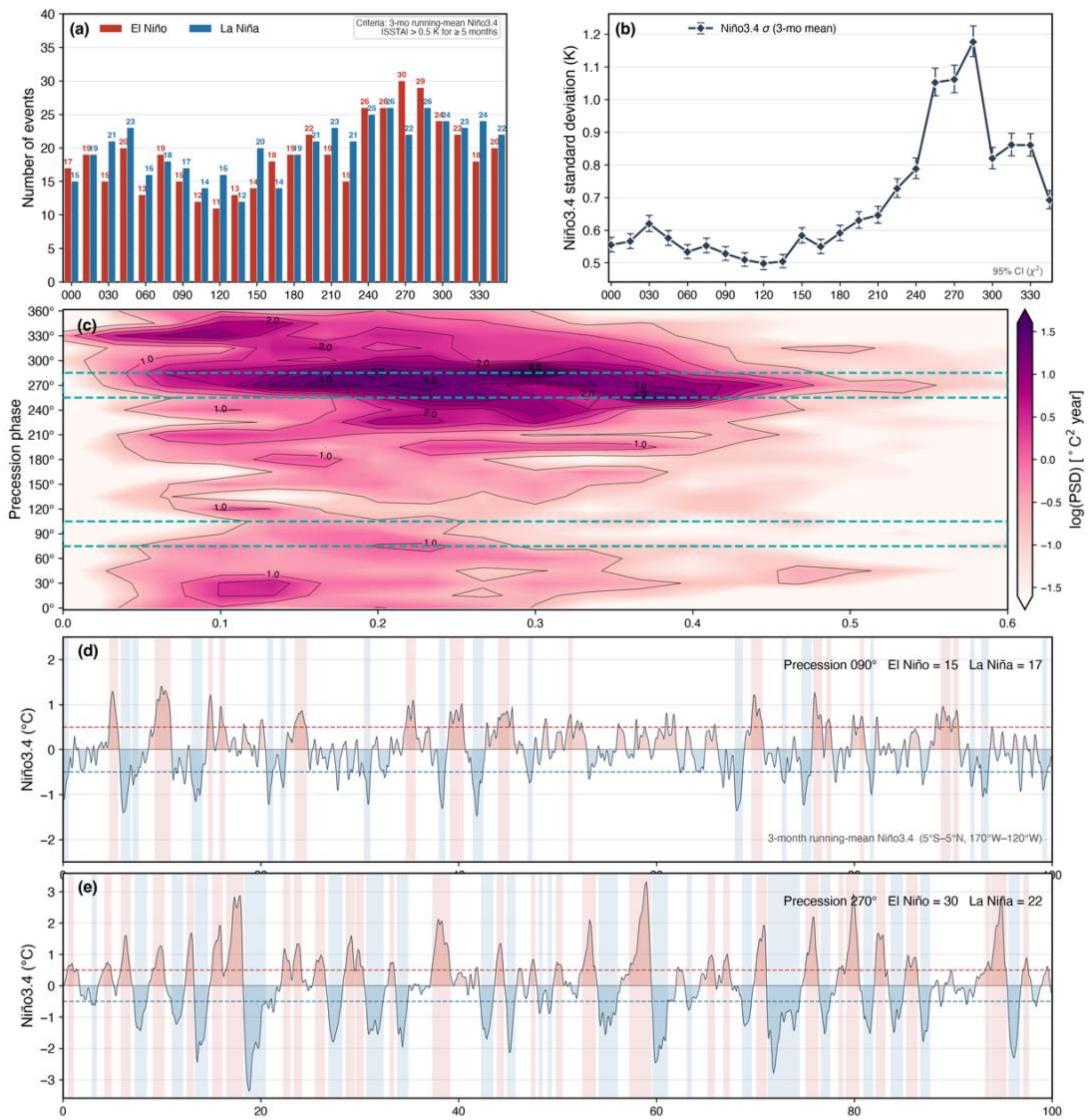

Fig. R19. Same ENSO diagnostics as Supplementary Fig. S3 but using the Niño3.4 index (5°S–5°N, 170°W–120°W).

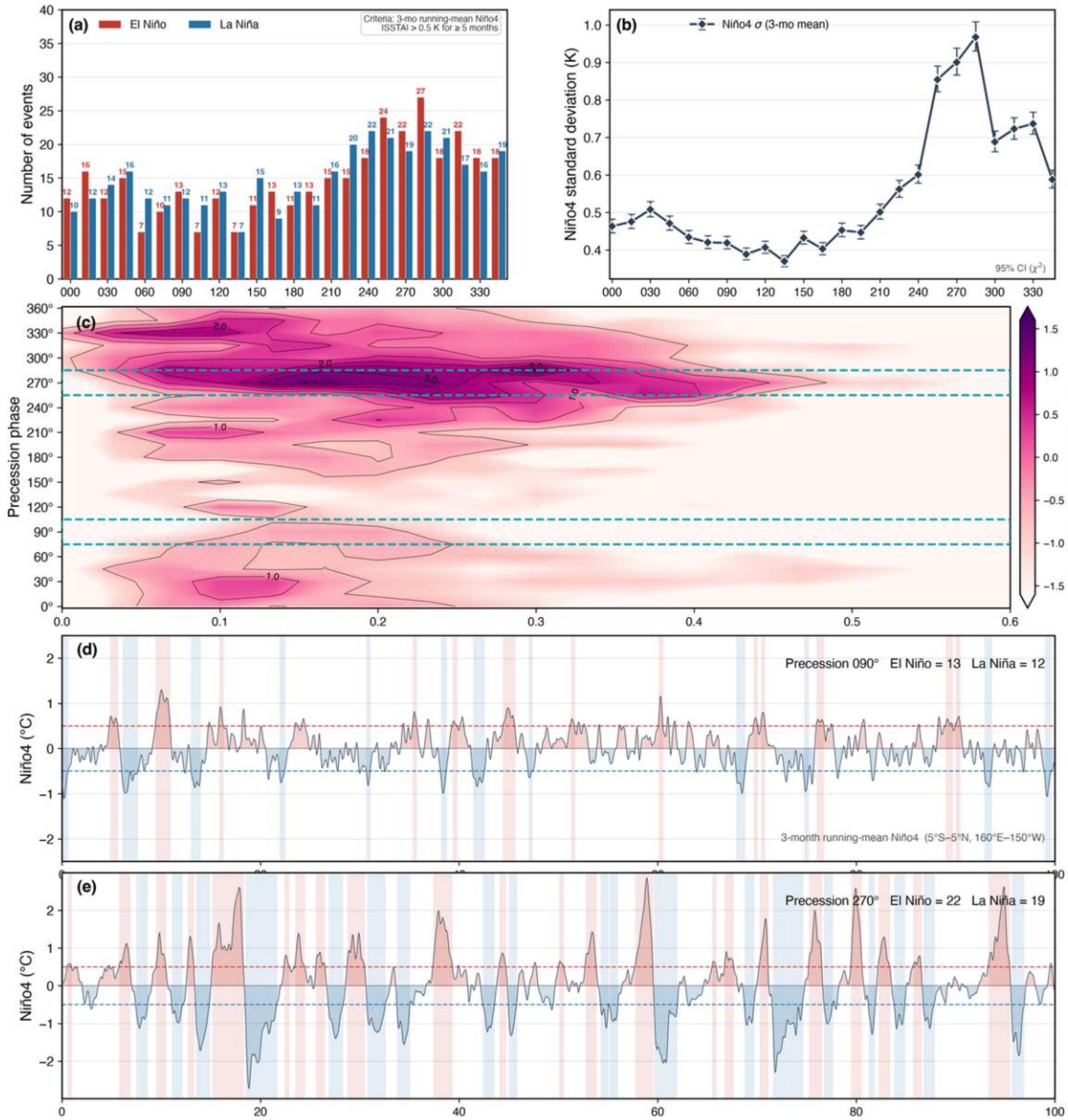

Fig. R20. Same ENSO diagnostics as Supplementary Fig. S3, but using the Niño4 index (5°S–5°N, 160°E–150°W).

Therefore, Niño3 was selected because it best captures the spatial maximum of simulated ENSO variability, but the inferred precessional modulation is independent of the specific ENSO index definition.

Lines 154–155 (Methods): *"Sensitivity tests using the Niño3.4 and Niño4 regions (not shown) confirm that the main conclusions are insensitive to the choice of ENSO index region. "*

The authors cite Yang et al. 2024 for model "experimental settings", but it would be helpful to include pCO2 and other greenhouse gas levels, alongside information related to obliquirt and other boundary conditions as well.

REPLY: In the revised manuscript, we have added a detailed description of the key boundary conditions of the 24 precession sensitivity experiments in the Methods section, thereby improving the description of the experimental design rather than relying solely on Yang et al. (2024). Specifically, all experiments were conducted under fixed near-preindustrial boundary conditions. Atmospheric greenhouse-gas concentrations were prescribed as CO_2 = 284.32 ppm, CH_4 = 808.25 ppb, and N_2O = 273.02 ppb, while land–sea distribution and ice-sheet extent were kept unchanged. For orbital parameters, eccentricity was fixed at 0.058 and obliquity at 24.50°, with only the longitude of perihelion varied to represent a complete precessional cycle. The precessional phase was varied from 0° to 345° at 15° intervals, with 90° and 270° corresponding to perihelion at the boreal and austral summer solstices, respectively. Each simulation was integrated for 400 years, and the final 100 years after climate equilibration were used for subsequent ENSO and mean-state analyses.

Lines 119–136 (Methods): *" Previous paleoclimate reconstructions and numerical simulations often considered multiple external forcings, making it difficult to isolate the specific role of individual factors. To specifically assess the impact of precession on ENSO activity, we conducted 24 time-slice simulations reconstructing a full precessional cycle using the Alfred Wegener Institute Earth System Model (AWI-ESM) (Sidorenko et al., 2015). The precessional phase was varied from 0° to 345° in 15° increments. In this framework, a precessional phase of 90° corresponds to perihelion at the boreal summer solstice, whereas a phase of 270° corresponds to perihelion at the austral summer solstice. Each simulation was integrated for 400 years. After the tropical climate had equilibrated, the final 100 years were used for the ENSO and mean-state analyses presented in this study. This design allows us to systematically assess ENSO characteristics under varying seasonal distributions of insolation driven by precession (Milankovitch, 1941). The main boundary conditions of the 24 experiments are as follows. Greenhouse-gas concentrations, land–sea distribution, and ice-sheet extents were held fixed at pre-industrial conditions. Orbital parameters were prescribed with eccentricity fixed at 0.058 to amplify the precessional insolation contrast, consistent with previous idealized orbital experiments (Yang et al., 2025), and obliquity fixed at 24.50°; only the longitude of perihelion was varied across the 24 time slices. All other boundary conditions follow the AWI-ESM configuration described by Yang (2024)."*

The authors should specify the duration of each timeslice used for ENSO calculations, the number of independent ENSO events sampled, and include explicit uncertainty estimates for ENSO variance.

REPLY: We have added the requested analyses to the Methods and Results sections and updated Supplementary Figure S3 accordingly. Specifically, we now explicitly describe the analysis period for each precessional experiment, quantify ENSO event occurrence, and provide uncertainty estimates for ENSO variance.

Lines 148–161 (Methods): *"To evaluate ENSO variability across precessional phases, we first examine the longitude–precession distribution of equatorial Pacific sea surface temperature (SST) anomaly (SSTA) standard deviation (Figure 1a). Interannual variance is largest in the eastern equatorial Pacific; therefore, we use the Niño3 region (5°S–5°N, 150°W–90°W) as the primary ENSO index (Trenberth, 2001). Monthly SST anomalies are calculated relative to each experiment's climatological seasonal cycle over the final 100 years after removing linear trends. The Niño3 index is defined as the three-month running mean of Niño3 SST anomalies. Sensitivity tests using the Niño3.4 and Niño4 regions (not shown) confirm that the main conclusions are insensitive to the choice of ENSO index region. ENSO amplitude is quantified as the standard deviation of the Niño3 index, with 95% confidence intervals estimated from the chi-square distribution (Supplementary Figure S3b). El Niño and La Niña events are identified when the three-month running-mean Niño3 SSTA exceeds +0.5 K or falls below −0.5 K for at least five consecutive overlapping three-month periods (Supplementary Figure S3a, d,e). Power spectral analysis of the Niño3 index is used to characterize ENSO frequency (Supplementary Figure S3c). For the representative weak and strong precessional phases (90° and 270°), we also perform lead–lag correlation and El Niño composite analyses to examine ENSO life-cycle evolution. These event-scale diagnostics characterize differences in ENSO evolution and coupled ocean–atmosphere feedback between the 270° and 90° phases (figures not reproduced here). "*

Lines 229–241 (Results): *" In addition, precession influences not only ENSO amplitude but also ENSO frequency and event occurrence (Supplementary Figure S3). Across the 24 experiments, both El Niño and La Niña events occur more frequently near 255°–300° and less frequently near 75°–135° (Supplementary Figure S3a). In the representative weak and strong phases, the 90° experiment yields 19 El Niño and 19 La Niña events, whereas the 270° experiment yields 31 and 25 events, respectively. Power spectra likewise indicate a shift toward shorter ENSO timescales near 255°–300°, with the dominant spectral peak shifting from approximately a 6-year period at 90° to approximately a 4-year period at 270° (Supplementary Figure S3c). The corresponding Niño3 time series illustrate this contrast, with more frequent and larger-amplitude events under the 270° phase than under the 90° phase (Supplementary Figure S3d,e). Together, these results demonstrate that precession coherently modulates both ENSO amplitude and frequency (Lu et al., 2025). To understand this response, we next examine how precession reorganizes the tropical Pacific mean state."*